



Spectroscopy[®]

Solutions for Materials Analysis

June 2018 Volume 33 Number 6

www.spectroscopyonline.com

NIR Analysis of Tobacco

**Evaluating the Temperature-Dependent
Raman Spectra of Amorphous
Polyethylene Terephthalate**

**Quantifying Metal Concentrations
in Single Cells with ICP-MS**

**A Review of Calibration
Transfer Chemometrics**

UNLOCK THE UNKNOWN

ASK

**APPLIED
SPECTRAL
KNOWLEDGE**

Equipping people to solve the greatest challenges
in health, safety and the environment.



www.oceanoptics.com

info@oceanoptics.com • US +1 727-733-2447 • EUROPE +31 26-3190500 • ASIA +86 21-6295-6600

State-of-the-Art X-Ray Solutions

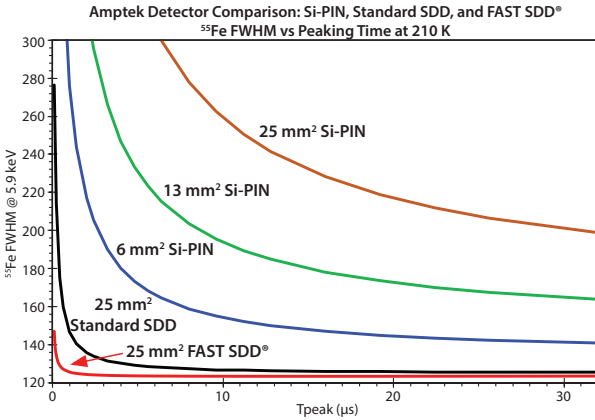
•FAST SDD®

•SDD

•Si-PIN

In-house manufacturing = The highest performing detectors available

The best detector for optimal results



FAST SDD® Detector

>2,000,000 CPS and 122 eV FWHM Resolution

Options:

- 25 mm² collimated to 17 mm²
- 70 mm² collimated to 50 mm²
- Windows: Be (0.5 mil) 12.5 μm, or C Series (Si₃N₄)
- TO-8 package fits all Amptek configurations

Configurations to meet your needs



XR-100 and PX5 Digital Pulse Processor

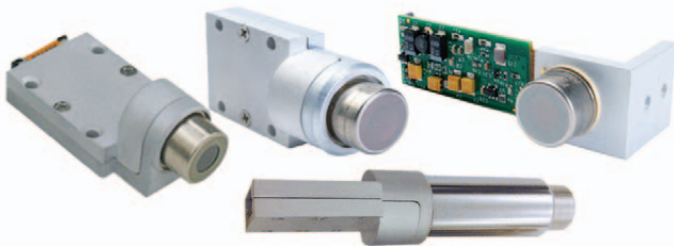


X-123 Complete X-Ray Spectrometer



XRF Experimenters Kit

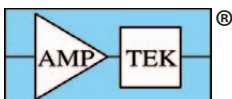
OEM Configurations



A sample of detectors with preamplifiers and heat sinks



Digital Pulse Processors and Power Supplies



OEM's #1 Choice
For XRF

amptek.com



Spectroscopy®

MANUSCRIPTS: To discuss possible article topics or obtain manuscript preparation guidelines, contact the editorial director at: (732) 346-3020, e-mail: Laura.Bush@ubm.com. Publishers assume no responsibility for safety of artwork, photographs, or manuscripts. Every caution is taken to ensure accuracy, but publishers cannot accept responsibility for the information supplied herein or for any opinion expressed.

SUBSCRIPTIONS: For subscription information: *Spectroscopy*, P.O. Box 6196, Duluth, MN 55806-6196; (888) 527-7008, 7:00 a.m. to 6:00 p.m. CST. Outside the U.S., +1-218-740-6477. Delivery of *Spectroscopy* outside the U.S. is 3–14 days after printing. Single-copy price: U.S., \$10.00 + \$7.00 postage and handling (\$17.00 total); Canada and Mexico, \$12.00 + \$7.00 postage and handling (\$19.00 total); Other international, \$15.00 + \$7.00 postage and handling (\$22.00 total).

CHANGE OF ADDRESS: Send change of address to *Spectroscopy*, P.O. Box 6196, Duluth, MN 55806-6196; provide old mailing label as well as new address; include ZIP or postal code. Allow 4–6 weeks for change. Alternately, go to the following URL for address changes or subscription renewal: <http://ubmsubs.ubm.com/?pubid=SPEC>

RETURN ALL UNDELIVERABLE CANADIAN ADDRESSES TO: IMEX Global Solutions, P.O. Box 25542, London, ON N6C 6B2, CANADA. PUBLICATIONS MAIL AGREEMENT No.40612608.

REPRINT SERVICES: Reprints of all articles in this issue and past issues are available (500 minimum). Licensing and Reuse of Content: Contact our official partner, Wright's Media, about available usages, license fees, and award seal artwork at advanstar@wrightsmedia.com for more information. Please note that Wright's Media is the only authorized company that we've partnered with for Advanstar UBM materials.

C.A.S.T. DATA AND LIST INFORMATION: Contact Melissa Stillwell, (218) 740-6831; e-mail: Melissa.Stillwell@ubm.com

INTERNATIONAL LICENSING: Jillyn Frommer, (732) 346-3007, fax: (732) 647-1104; e-mail: Jillyn.Frommer@ubm.com

485F US Highway One South, Suite 210
Iselin, NJ 08830
(732) 596-0276
Fax: (732) 647-1235

Michael J. Tessalone

Vice President/Group Publisher
Michael.Tessalone@ubm.com

Stephanie Shaffer

Publisher
Stephanie.Shaffer@ubm.com

Edward Fantuzzi

Associate Publisher
Edward.Fantuzzi@ubm.com

Michael Kushner

Senior Director, Digital Media
Michael.Kushner@ubm.com

Laura Bush

Editorial Director
Laura.Bush@ubm.com

Megan L'Heureux

Managing Editor
Meg.L'Heureux@ubm.com

Stephen A. Brown

Group Technical Editor
Stephen.Brown@ubm.com

Cindy Delonas

Associate Editor
Cindy.Delonas@ubm.com

Kristen Moore

Webcast Operations Manager
Kristen.Moore@ubm.com

Vania Oliveira

Project Manager
Vania.Oliveira@ubm.com

Sabina Advani

Digital Production Manager
Sabina.Advani@ubm.com

Kaylynn Chiarello-Ebner

Managing Editor, Special Projects
Kaylynn.Chiarello.Ebner@ubm.com

Dan Ward

Art Director
dward@hcl.com

Anne Lavigne

Marketing Manager
Anne.Lavigne@ubm.com

Melissa Stillwell

C.A.S.T. Data and List Information
Melissa.Stillwell@ubm.com

Thomas W. Ehardt

Executive Vice-President, Senior Managing Director
UBM Life Sciences Group

Dave Esola

VP & General Manager
UBM Life Sciences Group

Jillyn Frommer

Permissions
Jillyn.Frommer@ubm.com

Jesse Singer

Production Manager
jsinger@hcl.com

Wendy Bong

Audience Development Manager
Wendy.Bong@ubm.com

Ross Burns

Audience Development Assistant Manager
Ross.Burns@ubm.com



© 2018 UBM. All rights reserved. No part of this publication may be reproduced or transmitted in any form or by any means, electronic or mechanical including by photocopy, recording, or information storage and retrieval without permission in writing from the publisher. Authorization to photocopy items for internal/educational or personal use, or the internal/educational or personal use of specific clients is granted by UBM for libraries and other users registered with the Copyright Clearance Center, 222 Rosewood Dr. Danvers, MA 01923, 978-750-8400 fax 978-646-8700 or visit <http://www.copyright.com> online. For uses beyond those listed above, please direct your written request to Permission Dept. fax 732-647-1104 or email: Jillyn.Frommer@ubm.com.

UBM Americas provides certain customer contact data (such as customers' names, addresses, phone numbers, and e-mail addresses) to third parties who wish to promote relevant products, services, and other opportunities that may be of interest to you. If you do not want UBM Americas to make your contact information available to third parties for marketing purposes, simply call toll-free 866-529-2922 between the hours of 7:30 a.m. and 5 p.m. CST and a customer service representative will assist you in removing your name from UBM Americas lists. Outside the U.S., please phone 218-740-6477.

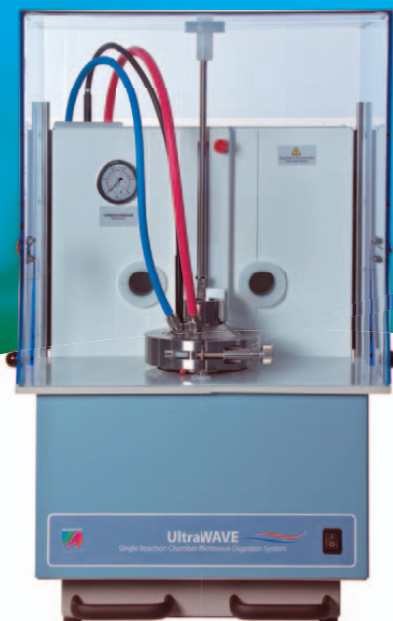
Spectroscopy does not verify any claims or other information appearing in any of the advertisements contained in the publication, and cannot take responsibility for any losses or other damages incurred by readers in reliance of such content.

Spectroscopy welcomes unsolicited articles, manuscripts, photographs, illustrations and other materials but cannot be held responsible for their safekeeping or return.

To subscribe, call toll-free 888-527-7008. Outside the U.S. call 218-740-6477.

UBM Americas (www.ubmamericas.com) is a leading worldwide media company providing integrated marketing solutions for the Fashion, Life Sciences and Powersports industries. UBM Americas serves business professionals and consumers in these industries with its portfolio of 91 events, 67 publications and directories, 150 electronic publications and Web sites, as well as educational and direct marketing products and services. Market leading brands and a commitment to delivering innovative, quality products and services enables UBM Americas to "Connect Our Customers With Theirs." UBM Americas has approximately 1000 employees and currently operates from multiple offices in North America and Europe.

Envelope pushed. Game changed.



Improved workflow

At least 2X the throughput

No batching required

Lower operating costs

You'll never look at metals prep the same way again.

The Milestone UltraWAVE isn't just an evolution; it's a revolution—changing how industrial and research laboratories around the world prep samples for analysis.

Patented UltraWAVE Single Reaction Chamber (SRC) technology goes beyond traditional closed and open vessel digestion, offering significantly greater digestion capabilities for even the most difficult sample types.

High-performance stainless steel construction allows for higher pressures and temperatures, while disposable vessels eliminate the need to assemble, disassemble or clean between processing. Just as important, dissimilar samples can be processed simultaneously, saving time and money. The bottom line? The UltraWAVE is changing the game for metals prep.

Download a **FREE Milestone LabNote™**

No Limits: How SRC Technology is Changing the Game for Metals Prep
at milestonesci.com/gamechanger



Ethos EZ



UltraWAVE



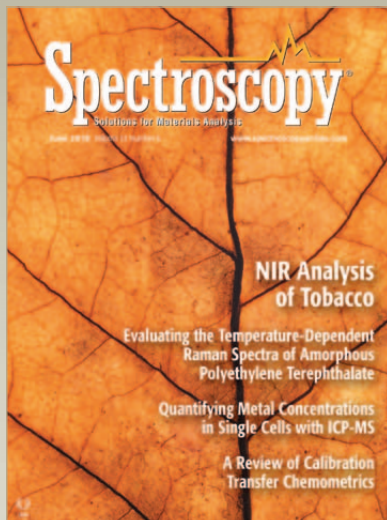
UltraCLAVE



Spectroscopy

June 2018

Volume 33 Number 6



Cover image courtesy of
Vladimir A Veljanovski / shutterstock.com

ON THE WEB

WEB SEMINARS

How MS/MS Can Improve Your ICP-MS Data Quality, Whatever Your Application

Bert Woods, Agilent Technologies

Improving the Elemental Analysis of Polymers and Plastics Using XRF

Dirk Wissman,
SPECTRO Analytical Instruments

Illuminating LA-ICP-MS: Direct Solid Analysis and Exciting New Opportunities

Daniel Kutscher and Dr. Dhinesh Asogan,
Thermo Fisher Scientific

Exploring Four Capabilities that are Defining the Future of ICP-MS

Abelardo Gutierrez, Agilent Technologies
spectroscopyonline.com/spec/webcasts

Like *Spectroscopy* on Facebook:
www.facebook.com/SpectroscopyMagazine



Follow *Spectroscopy* on Twitter:
<https://twitter.com/spectroscopyMag>



Join the *Spectroscopy* Group on LinkedIn
<http://linkd.in/SpecGroup>



CONTENTS

COLUMNS

Molecular Spectroscopy Workbench 12

2D COS of Temperature-Dependent Raman Spectra of Amorphous, Nonoriented Polyethylene Terephthalate to Separate Molecular Conformational Changes from True Crystallization

Fran Adar

Because of the structural use of polymers, it is important to understand the origin of their strength, elongation to break, elasticity, flexibility, and so on. It is in the very low frequency region (the so called "terahertz" range) where it is believed that the real indicators for crystallinity appear.

Chemometrics in Spectroscopy 22

Calibration Transfer Chemometrics, Part II: A Review of the Subject

Jerome Workman Jr. and Howard Mark

Calibration transfer involves several strategies and mathematical techniques for applying a single calibration database consisting of samples, reference data, and calibration equations to two or more instruments. In this installment, we review the chemometric and tactical strategies used for the calibration transfer process.

PEER-REVIEWED ARTICLES

Exploring the Applicability of Quantitative Models Based on NIR Reflectance Spectroscopy of Plant Samples 27

Yuqing Yang, Li Ma, Guorong Du, Junhui Li, and Yanjun Ma

The establishment of quantitative models based on the near-infrared (NIR) spectroscopic analysis of plant samples plays an important role in improving both the scope of the models and the accuracy of prediction. This technique could provide a new method for tobacco quality management and provide a new discriminant method for other agricultural products.

Single-Cell ICP-MS Analysis: Quantifying the Metal Concentration of Unicellular Organisms at the Cellular Level 33

Ruth Merrifield, Lauren Amable, and Chady Stephan

Single-cell ICP-MS can accurately quantify the metal concentrations within individual cells, providing new information about the mean metal content and the variation within a cell population. This method is shown to be a vital tool for assessing the specific uptake of metals by ovarian cancer cells and fresh water algae.

DEPARTMENTS

News Spectrum	10
Vendor Perspectives	40
Products & Resources	44
Ad Index	46

Spectroscopy (ISSN 0887-6703 [print], ISSN 1939-1900 [digital]) is published monthly by UBM LLC 131 West First Street, Duluth, MN 55802-2065. *Spectroscopy* is distributed free of charge to users and specifiers of spectroscopic equipment in the United States. *Spectroscopy* is available on a paid subscription basis to nonqualified readers at the rate of: U.S. and possessions: 1 year (12 issues), \$74.95; 2 years (24 issues), \$134.50. Canada/Mexico: 1 year, \$95; 2 years, \$150. International: 1 year (12 issues), \$140; 2 years (24 issues), \$250. Periodicals postage paid at Duluth, MN 55806 and at additional mailing offices. POSTMASTER: Send address changes to *Spectroscopy*, P.O. Box 6196, Duluth, MN 55806-6196. PUBLICATIONS MAIL AGREEMENT NO. 40612608, Return Undeliverable Canadian Addresses to: IMEX Global Solutions, P. O. Box 25542, London, ON N6C 6B2, CANADA. Canadian GST number: R-124213133RT001. Printed in the U.S.A.



Maximizing the return-on-investment for the refining & petrochemical industries

TALYS ASP400

TALYS ASP400 series is a single-point fiber optics based industrial FT-NIR analyzer designed to make in-line monitoring and control of continuous processes easy. Its simple installation enables real-time process monitoring, determination of stream properties or physical qualities, process characterization and early troubleshooting. The embedded Ex Area purge controller provides full connectivity to DCS: Modbus TCP/IP, RTU and OPC. With virtually no scheduled maintenance for 5-years, it delivers a low total cost of ownership. Learn more at abb.com/analytical or contact us at ftir@ca.abb.com



Editorial Advisory Board

Fran Adar Horiba Scientific

Russ Algar University of British Columbia

Matthew J. Baker University of Strathclyde

Ramon M. Barnes University of Massachusetts

Mathieu Baudelet University of Central Florida

Rohit Bhargava University of Illinois at Urbana-Champaign

Paul N. Bourassa Blue Moon Inc.

Michael S. Bradley Thermo Fisher Scientific

Deborah Bradshaw Consultant

Lora L. Brehm The Dow Chemical Company

George Chan Lawrence Berkeley National Laboratory

John Cottle University of California Santa Barbara

David Lankin University of Illinois at Chicago,
College of Pharmacy

Barbara S. Larsen DuPont Central Research and Development

Bernhard Lendl Vienna University of Technology (TU Wien)

Ian R. Lewis Kaiser Optical Systems

Rachael R. Ogorzalek Loo University of California Los Angeles,
David Geffen School of Medicine

Howard Mark Mark Electronics

R.D. McDowall McDowall Consulting

Gary McGeorge Bristol-Myers Squibb

Linda Baine McGown Rensselaer Polytechnic Institute

Francis M. Mirabella Jr. Mirabella Practical Consulting Solutions, Inc.

Ellen V. Miso Illuminate

Michael L. Myrick University of South Carolina

John W. Olesik The Ohio State University

Steven Ray State University of New York at Buffalo

Jim Rydzak Specere Consulting

Jerome Workman Jr. Unity Scientific

Lu Yang National Research Council Canada

Spectroscopy's Editorial Advisory Board is a group of distinguished individuals assembled to help the publication fulfill its editorial mission to promote the effective use of spectroscopic technology as a practical research and measurement tool. With recognized expertise in a wide range of technique and application areas, board members perform a range of functions, such as reviewing manuscripts, suggesting authors and topics for coverage, and providing the editor with general direction and feedback. We are indebted to these scientists for their contributions to the publication and to the spectroscopy community as a whole.



MA-3 Solo Direct Combustion Hg Analyzer

The applications and demand for thermal decomposition mercury measurements are expanding due to the amendment of laws and regulations regarding mercury measurement. In response to this trend, Nippon Instruments Corporation has released a new thermal decomposition mercury analyzer that meets the needs of the times and boasts excellent cost performance.

Affordable, High-performance Direct Mercury Analysis

- USEPA 7473
- ASTM D 6722-01
- ASTM D 7623-10
- UOP 1009-15
- JIS K0102



Nippon Instruments Corporation

Osaka office 14-8 Akaoji-cho, Takatsuki-shi, Osaka 569-1146 Japan
/Tech. center: TEL +81-72-694-5195 FAX +81-72-694-0663
E-mail hg-nic@rigaku.co.jp URL www.hg-nic.com

Singapore office: 10 Science Park Road, #03-24A, Singapore 117684
TEL +65-6873-7068 FAX +65-6873-6372



the
**NEXT
GENERATION**

ConcentratIR2™



A high-precision multiple reflection ATR accessory measuring only 18.5 cubic inches. Designed for microliter sampling. Compact enough to fit any spectrometer.

Choice of diamond or silicon ATR crystals.
Flow and heated options available.



harricksci.com/ConcentratIR2

News Spectrum

PerkinElmer Acquires Shanghai Spectrum Instruments

PerkinElmer (Waltham, Massachusetts), a provider of diagnostics, analytical solutions, and analytical instruments, has acquired Shanghai Spectrum Instruments Company (SSI) (Shanghai, China). SSI is a manufacturer of analytical instruments in China. The company provides analytical solutions and services to a range of research, academic, government, pharmaceutical, industrial, life sciences, and chemical analysis laboratories. Its portfolio includes photoelectric colorimeters, UV-vis spectrophotometers, atomic absorption spectrophotometers, and accessories.

Jim Corbett, an executive vice president and president at PerkinElmer said his company is committed to expanding its investment and manufacturing footprint in China. "This acquisition helps us build upon our China presence through SSI's strong, localized market position," he said. He added that the acquisition will enable PerkinElmer to reach a wider customer base throughout China and other emerging market regions.

SSI has customers in 10 countries, along with a supply chain and dealer network in China.

Investigation of the Use of LIBS to Quantitate Lead in Atmosphere

In a recent study (1), researchers investigated the use of laser-induced breakdown spectroscopy (LIBS) for the quantitative measurement of lead in aerosols, as an alternative to using inductively coupled plasma with optical emission spectroscopy or mass spectrometry (ICP-OES or ICP-MS).

Quantitative measurements with LIBS present several challenges. The study, by a team at CNR-ICMATE, the Institute of Condensed Matter Chemistry and Technologies for Energy in Italy, focused primarily on the investigating matrix effects, with a focus on the role of the carrier gas on the LIBS signal itself and the behavior of the LIBS signal as a function of the delay time with respect to the laser pulse.

The researchers found that for delay times higher than 50 μ s, the LIBS signal in air is substantially lower than the values obtained in nitrogen. At short delay times, the LIBS signal is enhanced in air compared to nitrogen. The researchers concluded that more work needs to be done to investigate the chemical kinetic mechanisms that may be responsible for the observed results.

Reference

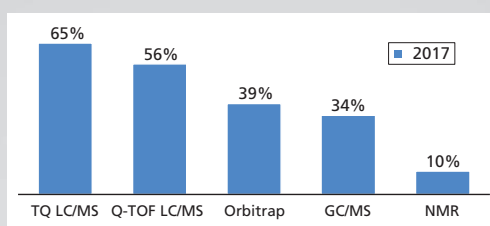
- (1) K.D.A. Redoglio, N. Palazzo, F. Migliorini, R. Donde, and S. De Iuliis, *Appl. Spectrosc.* **72**(4), 584–590 (2018).

MARKET PROFILE: METABOLOMICS

Metabolomics is one of the newer "omics" fields, and focuses on the characterization of the small molecule metabolites in biological systems. Metabolomics research has the potential to shed light on certain disease states, monitor patient response to treatment, and contribute to drug target discovery. Applications also span pharmaceutical development and neuroscience research.

The market for metabolomics analysis has seen significant growth in the past decade, but other "omics" areas such as proteomics and genomics still receive much more attention. The huge chemical diversity of metabolites and their transient nature make their identification and study difficult. Like proteomics, metabolomics is beginning to find a home in clinical applications. It will take time for diagnostic methods to become established, but this represents an example of how metabolomics is continuing to break into new fields.

In line with the growing popularity of the field, development of analytical systems capable of carrying out in-depth discoveries of the metabolome is on the rise. The market for the analytical systems and related products used for metabolomics is predicted to grow to \$1.1 billion in 2022. As well as



Frequently mentioned analytical instruments used for metabolomics research

significant market growth, funding for metabolomics research has also increased, with National Institutes of Health (NIH) grant funding rising from \$100 million in 2007 to \$900 million in 2017.

The most popular instruments for metabolomics analysis are triple quadrupole liquid chromatography–mass spectrometry (LC–MS) systems, which comprise about two-thirds of the market, according

to a recent survey of metabolomics researchers conducted by Top-Down Analytics (TDA). Other frequently mentioned technologies were quadrupole time-of-flight (Q-TOF), orbital ion trap, and gas chromatography–mass spectrometry (GC–MS) instruments. Approximately 10% of the respondents had direct access to a nuclear magnetic resonance (NMR) instrument in their laboratory.

Market size and growth estimates were adopted from TDA's market research report, "Metabolomics 2018: Charged with Massive Potential." For more information, contact Glenn Cudiamat, general manager, at (888) 953-5655 or glenn.cudiamat@tdaresearch.com. Glenn is a market research expert who specializes in scientific technologies used in lab and process industries.

SciX is presented by
Federation of Analytical
Chemistry and
Spectroscopy Societies
and its 14 Member
Organizations

American Chemical Society
Division of Analytical
Chemistry

AES Electrophoresis Society

American Society for Mass
Spectrometry

ANACHEM

Austrian Society of Analytical
Chemistry

CLIRSPEC

Coblentz Society

Council for Near Infrared
Spectroscopy

Infrared and Raman
Discussion Group

International Society of
Automation-Analysis
Division

North American Society for
Laser Induced Breakdown
Spectroscopy

Royal Society of Chemistry

Society for Applied
Spectroscopy

The Spectroscopical Society
of Japan (SPSJ)

NATIONAL MEETING

Society for Applied
Spectroscopy (SAS)

AES Electrophoresis Society

Coblentz Society



FACSS PRESENTS

THE GREAT SCIENTIFIC EXCHANGE

SCIX2018

THE PREMIER MEETING FOR ANALYTICAL CHEMISTRY AND ALLIED SCIENCES
ATLANTA MARRIOTT MARQUIS • ATLANTA, GEORGIA
OCTOBER 21 - 26, 2018

Home of International LIBS 2018



CALL FOR PAPERS

April 30: Deadline for Oral Submissions
July 31: Deadline for Poster Submissions

Conference Topics

Atomic Spectroscopy | Chemical Imaging | Chemometrics for
Spectroscopy | Fluorescence Spectroscopy | Forensic Sciences | Infrared
Spectroscopy | Laser Induced Breakdown Spectroscopy | Mass Spectrometry
Microscopy | Nanotechnology | Near Infrared Spectroscopy Raman
Spectroscopy | Spectroscopic Bioanalysis | Spectroscopic Process Analytical
Spectroscopic Pharmaceutical Analysis | Spectroscopy Applied to Food
Safety | Surface Plasmon Resonance Spectroscopy
Terahertz Spectroscopy

Special Topics for 2018

- Infectious Diseases
- Microplastics
- Food and Drug Safety



KEYNOTE SPEAKER

Matthew Savoca

NOAA Southwest Fisheries Science Center
and Hopkins Marine Station, Stanford University

*"On Polymer Seas: The Rising Tide of Plastic in the Ocean
and What to Do About It"*



Molecular Spectroscopy Workbench

2D COS of Temperature-Dependent Raman Spectra of Amorphous, Nonoriented Polyethylene Terephthalate to Separate Molecular Conformational Changes from True Crystallization

In our previous column we discussed the application of two-dimensional correlation spectroscopy (2D COS) to the temperature-dependent, polarized Raman spectra of polyethylene terephthalate (PET) fibers to get some insight into the conformational changes that occur as the material's morphology is changing. As indicated at the time, we are now going to show spectra that include the very low frequency region (the so called "terahertz" range) where it is believed that the real indicators for crystallinity appear. By applying the interpretation rules of 2D COS, we can determine the sequence of changes that occur as the polymer is crystallizing.

Fran Adar

After a discussion with Professor Noda, and under his recommendation, we decided this time to examine the temperature dependent behavior of amorphous, nonoriented polyethylene terephthalate (PET), because when looking at fibers it becomes difficult to disentangle the effects of orientation from crystallization. We prepared a fully amorphous bit of PET by melting a pellet in a nonstick frying pan and quenching it in ice water. The

rapid solidification of the material prevents crystallization that can only occur on a longer timescale.

Figure 1 shows the spectra of the amorphous material after the rapid quench, and "crystalline" material after a slow cool. Note that polymers are almost never 100% crystalline, and PET is never seen to be much more than 50% crystalline. A comparison of these spectra reminds us which bands are robust indicators of changes that have

been associated with crystallinity. In these spectra, however, we also see the low-frequency contributions. In the low-frequency region, shown in Figure 2, there are several spectral features. There is the strict Rayleigh scattering caused by “particles” much smaller than the laser wavelength; the spectral width does not change, but the scattering is so intense as to overwhelm the detector under the conditions that we used. Then there is “quasi-elastic” scattering that is centered around the laser wavelength but broadened by interactions with the material sample. In amorphous material there can also be scattering by acoustic phonons, but in crystalline solids that scattering is forbidden by the selection rule based on conservation of momentum in an ordered material. In amorphous materials, where order is lacking, scattering by acoustic modes is possible. This band, called the *boson*, is broad because the intensity at each wavenumber shift corresponds to the density of vibrational states at that energy; in fact, if one needs to determine the “true” boson peak, the spectrum has to be divided by the Bose factor ($n(\omega) + 1$). There is also the possibility of a longitudinal acoustic mode (LAM), which is also an acoustic mode but is described as an accordion-like motion in crystalline lamellae of polymers. Actually, I have not seen any reports of LAM modes in PET, and enquiries of Neil Everall and John Chalmers confirmed this. Other possibilities for low-frequency scattering include both rotational and translational motion of the chains (1), but in the case of PET, there cannot be translational phonons because there is only one chain per unit cell (2).

Raman Spectra of Amorphous and Crystalline PET

The spectra shown in Figures 1–5 are displayed several ways. Initially the full spectra (-300 to 1800 cm^{-1}) are displayed; note that the bands in the low-frequency region and the bands between 950 and 1200 cm^{-1} , as well as 1550 – 1750 cm^{-1} have been band fit because these bands have been shown to reflect the molecular configurations

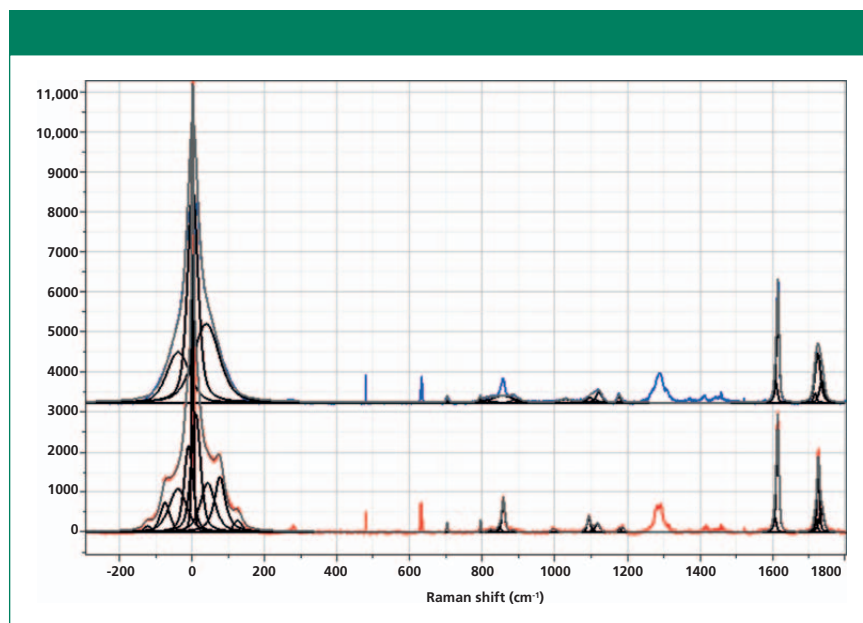


Figure 1: Raman spectra of amorphous, nonoriented sample of PET (top) versus crystalline nonoriented material (bottom).

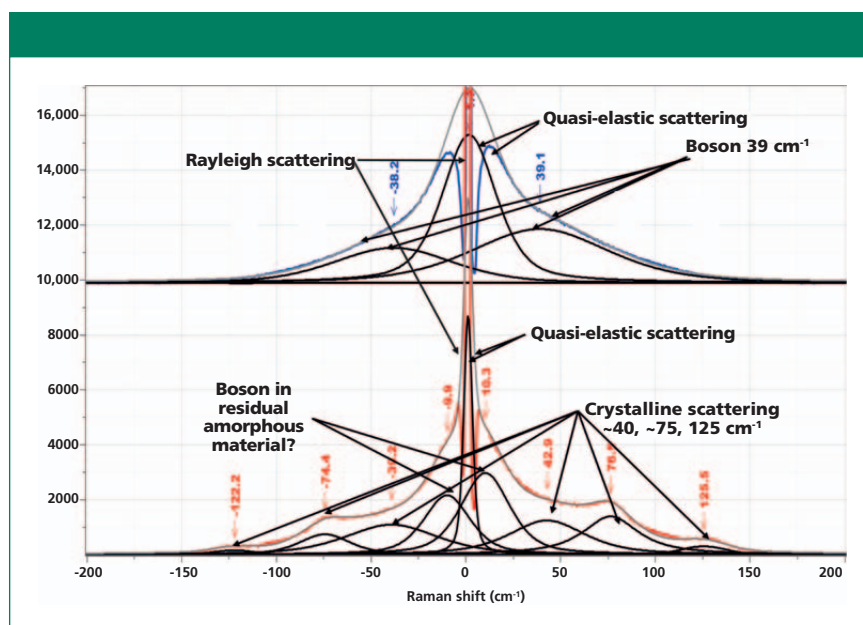


Figure 2: Low-frequency, Stokes–anti-Stokes Raman spectra of nonoriented amorphous (top) and nonoriented crystalline (bottom) PET.

that are consistent with the crystalline state. The second display shows the low-frequency region, and the remaining displays show the fingerprint region with varying enlargements to enhance the understanding of the changes. I have displayed the spectra this way because the low-frequency region is so intense that not much else can be seen easily in the full display.

The focus of this column is to de-

termine if, and how well, two-dimensional correlation (2D COS) Raman spectroscopy can provide these details without going to the effort of band-fitting, whose results are known to be non-unique in many cases.

The rigorous definition of crystallinity is uniform packing with translational symmetry. For polymers this requires uniform conformation of the chains. Relying on the discussion in

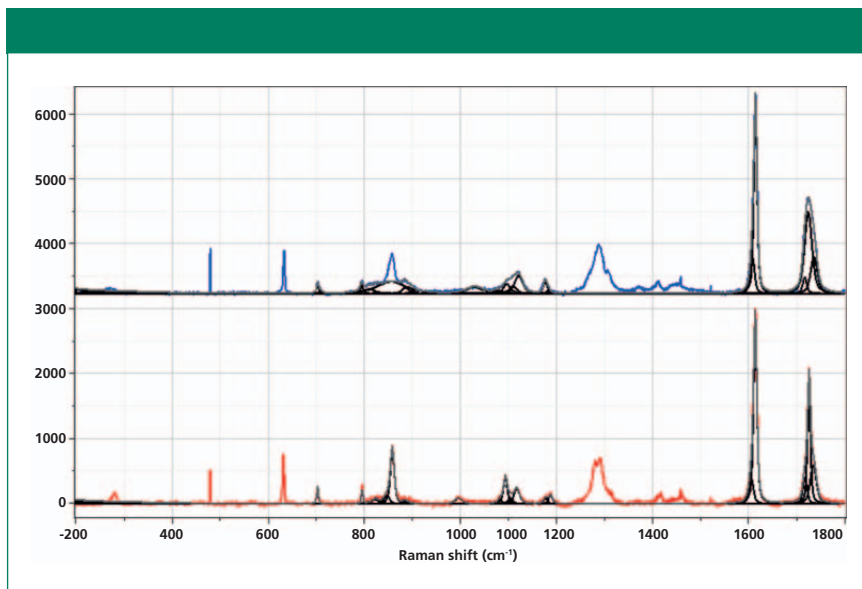


Figure 3: Fingerprint and aromatic-carbonyl regions of the Raman spectra of nonoriented amorphous (top) and crystalline (bottom) PET. The regions where bands have been associated with morphological changes have been band-fit and the following two figures will show the results of band-fitting more clearly.

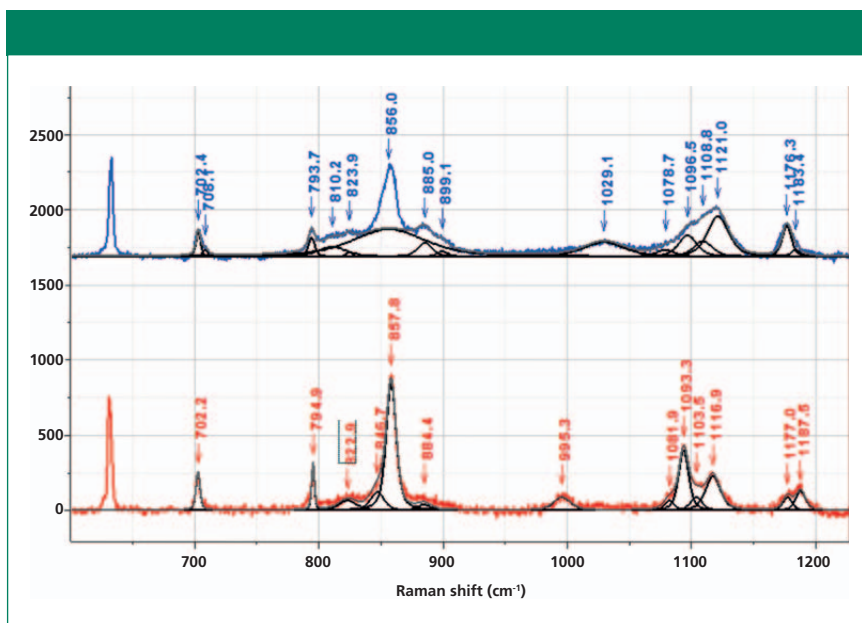


Figure 4: Fingerprint region of the Raman spectra of nonoriented amorphous (top) and crystalline (bottom) PET. The regions where bands have been associated with morphological changes have been band-fit.

the textbook by Bower and Maddams (3), who cite Zerbi, Ciampelli, and Zamboni's definitions for regularity peaks, we can begin to differentiate different morphological states. Zerbi and colleagues define three types of regularity peaks: peaks assigned to conformational regularity (that is, trans versus gauche rotational isomer-

ism) that can occur in both the solid and melt or solution but with varying relative intensities; the misnamed "crystallinity" peaks arising from long stereoregular chains; and then true crystallinity peaks that directly reflect interchain interactions. Although specific peaks in the spectra of polymers have been well correlated with crys-

tallinity (such as by correlating with density), if one does not understand the true nature of the vibration represented by a particular spectral band, the correlation may yield misleading results under some circumstances. Specifically in the case of PET, the carbonyl ($>C=O$) peak has been correlated with crystallinity following the 1972 article by Melveger (4). However, even Melveger stated that "the assumption of constant amorphous density in oriented samples may not be valid," which he knew would invalidate his method; in fact, the oriented, amorphous (mesomorphic) polymer would have different density than a randomly oriented amorphous sample.

I will be citing band assignments from the literature that have been helpful in characterizing PET morphology. However, to extract the maximum of information, one needs to fit the bands in the spectra (which itself is an operation that does not always yield unique results). The hope is that similar information can be extracted using 2D COS with much less work, and in addition, that the possibility for introducing artifacts from band-fitting will be avoided. Another important advantage is that bands that do not separate spectrally may separate in the 2D COS plots.

Spectral Interpretations and What to Look for in 2D COS

I know of only two publications showing spectra of the low-frequency behavior of PET in the literature (1,5). Bulkin and colleagues (1) note that the normal mode analysis by Boerio and colleagues (6), predicts B_g bands at 119 and 61 cm^{-1} that are derived from a twisting motion between the carbonyl carbon and the aromatic ring, and twisting about the same carbonyl carbon and the ester oxygen atom. In fact, the Boerio publication also predicts a third mode at 35 cm^{-1} composed of a third combination of the same twisting motions. The spectra in Figure 2 clearly show that bands close to these values only occur in the crystalline state, presumably because the variety of conformations in the amorphous state would wash out any defined

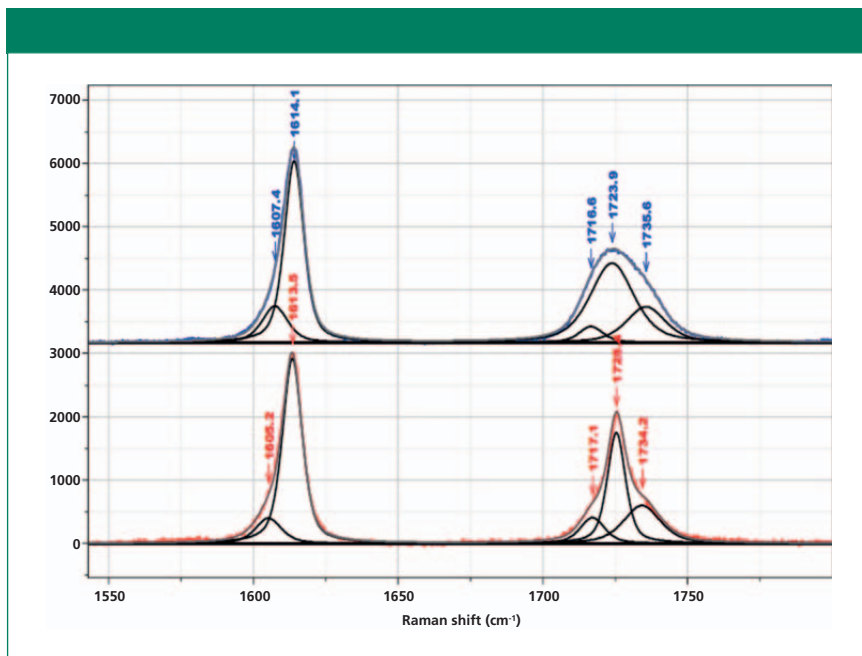


Figure 5: Raman spectrum in the region of the aromatic and carbonyl bands of nonoriented amorphous (top) and crystalline (bottom) PET, enlarged to provide better detail of the fitted bands, in particular the ones that have been associated with changes in morphology.

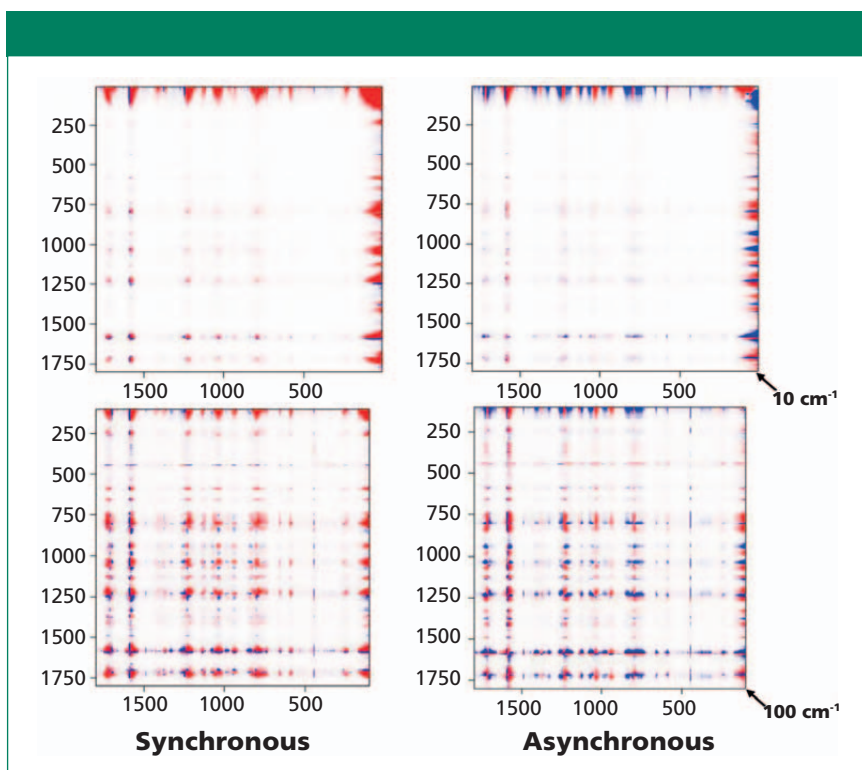


Figure 6: 2D COS of an amorphous sample that was followed as the temperature was raised from room temperature beyond T_g (~90 °C), to the melt at ~230 °C and then again at room temperature after a slow cool which enables the material to crystallize. Because of detector saturation in the Rayleigh line at 0 cm^{-1} these plots were started at 10 cm^{-1} (top) and 100 cm^{-1} (bottom).

peak. (The lowest frequency band is less obvious in the original spectra, but I added it to the fit to improve

the result—before I noticed the third low-frequency band in Boerio and colleagues original Table VIII [6]!)



art photonics
Broad Spectra Optical Fiber Solutions



Fiber probes for any spectroscopy method used in 0.2-16 μm range for clinical diagnostics

visit us at:

artphotonics.com

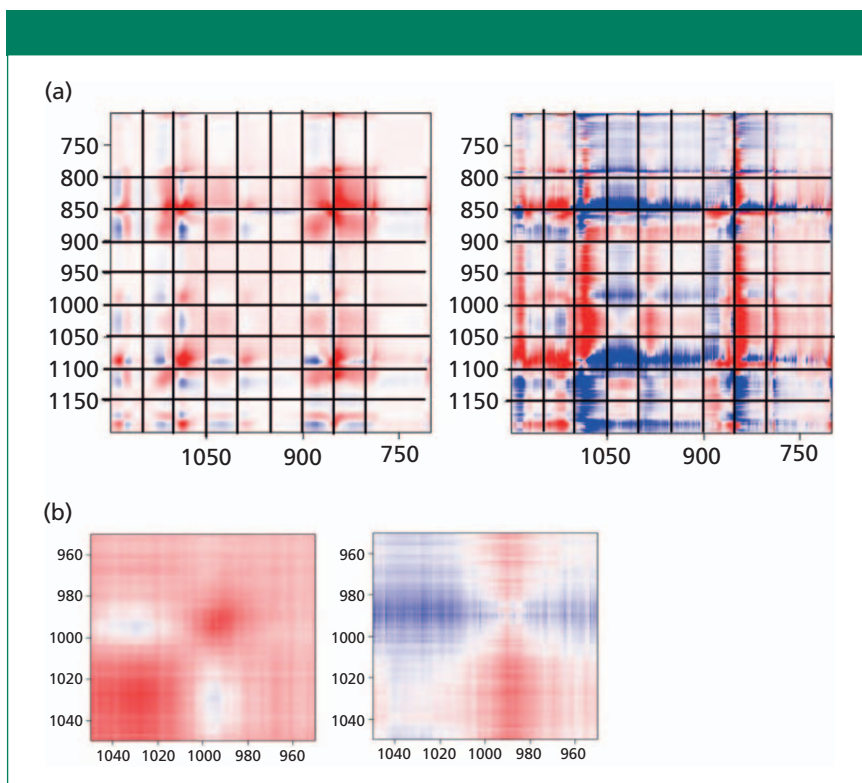


Figure 7: (a) Synchronous (left) versus asynchronous (right) in the region of the glycol bands where changes associated with “crystallization” are known to occur. (b) Synchronous (left) versus asynchronous (right) in the region of the glycol bands at 1000 cm^{-1} where changes associated with “crystallization” are known to occur.

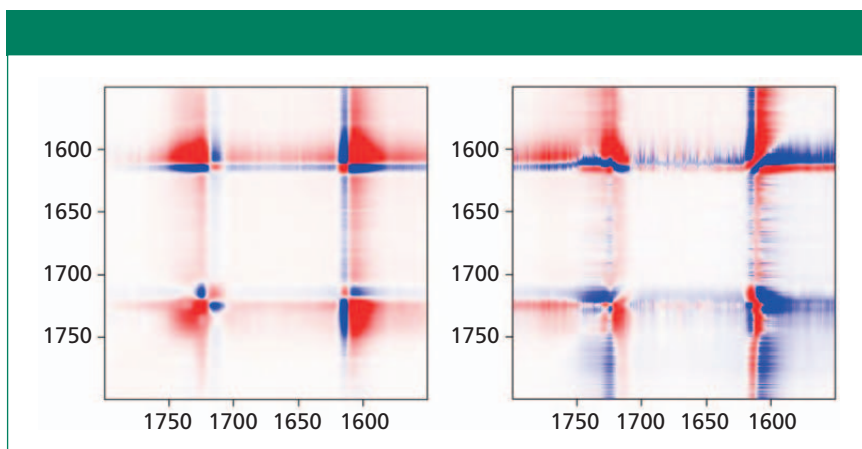


Figure 8: Synchronous (left) versus asynchronous (right) in the region of the aromatic ring and carbonyl bands where sharpening of the carbonyl is known to be associated with “crystallization.”

Now we want to examine more carefully the assignments of the “crystalline” sensitive bands in the fingerprint and carbonyl region to determine if 2D COSY can tell us the order in which the conformations change, relative to the low-frequency bands, and how that impacts crystallization. However, we need to remember that the low-frequency bands

do not directly reflect packing order (which is impossible in PET because there is only one chain in the unit cell), but still may be informative. Because the low-frequency “crystalline” bands that we are seeing presumably reflect the twisting motions determined by Boerio and colleagues (6), we may be able to argue that it is only when the chain is highly ordered that

these bands will emerge from the quasi-elastic scattering.

Inspection of the bands in the fingerprint/carbonyl region indicates that the biggest “crystallization”-sensitive change is the growth and sharpening of the central carbonyl band near 1725 cm^{-1} (Figure 5). There is actually much in the literature describing these changes. The carbonyl band can be fit by three components (7) (1716 and 1735 cm^{-1} , which are always broad, and 1725 cm^{-1} , which sharpens in the crystalline phase).

Possibly of more interest are the bands that reflect gauche to trans conformational changes because the crystalline regions require the trans conformation. Until recently, I believed that this was based on “reasonableness,” but in fact I found a publication in which 2D nuclear magnetic resonance (NMR) data were able to quantify the amounts of trans and gauche conformers and confirm that the crystalline form requires the trans conformation (8).

The bulk of the publications on Raman spectra of oriented PET (fibers and films) document the ability to measure orientation (by controlling polarization conditions) and gauche-trans transconformers by relying on normal mode analysis and changes that parallel the development of orientation, which require the trans conformation (7,9–13). The bands that have been recognized as gauche conformers (which will put kinks into the polymer chain in amorphous regions) are at 886 and 1030 cm^{-1} (9). Bands indicating the trans conformer are at 998 and 1096 cm^{-1} . The 998 cm^{-1} band is associated with O-CH₂ and C-C stretching of the glycol unit, and the 1096 cm^{-1} band has been assigned to a combination of the C-O stretch, the C-O-C bend, the C-C-O bend, and the C-C stretch (all motions also in the glycol unit). Both the 998 and 1096 cm^{-1} bands are markers for the crystalline conformation. The amorphous material has a broad band centered near 1120 cm^{-1} , with a shoulder near 1100 cm^{-1} from which the “crystal” contributions grow. I put “crystal” in quotes because we are trying to sep-

arate crystal effects from conformational effects, and the normal mode calculations were presumably done for the crystalline conformation known from X-ray diffraction (XRD).

The band-fit in the fingerprint region in Figure 4 allows one to follow the behavior of the bands identified as reflecting the trans versus gauche conformations. We confirm that the band at 886 cm^{-1} drops in intensity in the crystalline form, while the band at 995 cm^{-1} grows. In the region around 1100 cm^{-1} we see the growth of the trans band at 1096 cm^{-1} as well as other smaller features (such as a shoulder at 1080 cm^{-1}), some of which have been noticed by other workers (10). It would take a lot of work to sort out all of these small features using calculations, but by inspecting the 2D COS plots, we hope to see what is systematic, and even separate features that do not resolve spectrally because they are too close together. The plots that we will show were produced by 2D Shige (14) software available on the internet.

First-Level Use of 2D COS Results

2D COS software produces two two-dimensional plots of a set of spectra generated systematically by changing a variable that affects the spectrum. The two axes correspond to the wavelength (or wavenumber shift for Raman) that is spanned by the data. The synchronous plots, $\Phi(\nu_1, \nu_2)$ indicate which bands change simultaneously; note that simultaneous may mean in the same direction or in opposite directions. To be more explicit, if one species is converting to a second, the bands of the first species will decrease as the bands of the second increase. This change will be shown as two different colors in the 2D COS $\Phi(\nu_1, \nu_2)$ plot. The asynchronous plots, $\Psi(\nu_1, \nu_2)$, are a bit more difficult to understand, but can provide more information because they correlate sequential changes and responses from different origins. The asynchronous plot, $\Psi(\nu_1, \nu_2)$ will have no contributions for $\nu_1 = \nu_2$. What you do is compare $\Phi(\nu_1, \nu_2)$ to $\Psi(\nu_1, \nu_2)$. If the two have the same sign, then the

change occurs at ν_1 before ν_2 . If they have different signs, then the change occurs at ν_1 after ν_2 . In our case, we want to see if we can determine the order in which the changes occur in the glycol region, the carbonyl group, and the very low frequency region.

Figure 6 shows both the synchronous and the asynchronous plots for the full spectra of the melt-quenched sample which were measured as a function of temperature between room temperature and just above the

melt, and then again at room temperature after a slow cool that presumably yields a crystalline material. The intensities in red versus blue indicate that the output of the 2D COS calculation produces opposite signs at these points. To see more clearly what is in these plots, they will be enlarged in the regions of interest.

Figure 7 shows the 2D COS plots between 700 and 1200 cm^{-1} , Figure 8 between 1550 and 1800 cm^{-1} , and Figure 9 between 700 and 1200 cm^{-1}



Spectroscopy Sampling Solutions

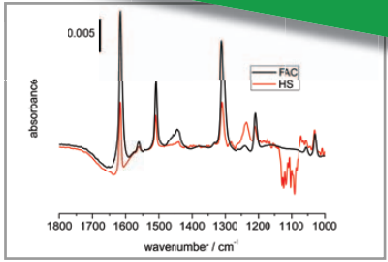
NEW Accessory Catalog!
Download at www.piketech.com

Featured Product

Spectroelectrochemistry with ATR-SEIRAS

The Jackfish Spectroelectrochemical Cell, designed to be coupled with the PIKE VeeMAX III, offers a complete out-of-the-box solution for surface-sensitive spectroelectrochemistry via ATR-SEIRAS technique. Such studies reveal fundamental details of electrochemical processes and provide information used in the development of next generation energy and sensing solutions.

ATR-SEIRAS relies on a Au thin film working electrode for surface-sensitivity. The Jackfish cell makes electrical contact with



Comparison of electrochemical ATR-SEIRAS response with the VeeMAX III Si 60 degree FAC (black) and a Si hemisphere (red).

PIKE VeeMAX III with Jackfish Cell



the film by using a unique spring-loaded pin design separated from the solution. This extends film lifetime and results in less time spent preparing Au films. High-quality infrared spectra can be obtained from submonolayer amounts of material at the electrode-solution interface. Using the VeeMAX III Si face-angled crystal (FAC), results can be obtained which outperform a conventional Si hemisphere in terms of signal-to-noise. Contact PIKE today to learn more.

PIKE TECHNOLOGIES (608) 274-2721
www.piketech.com
info@piketech.com

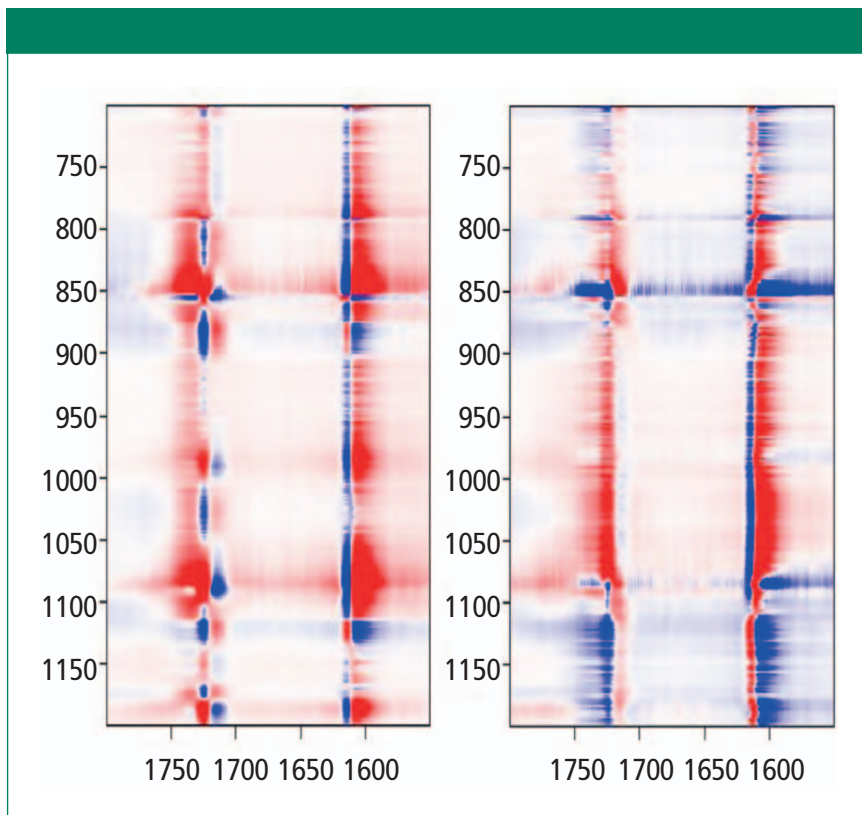


Figure 9: Synchronous (left) versus asynchronous (right) 2D COS in the heteroregion, crossing the glycol behavior with the carbonyl behavior.

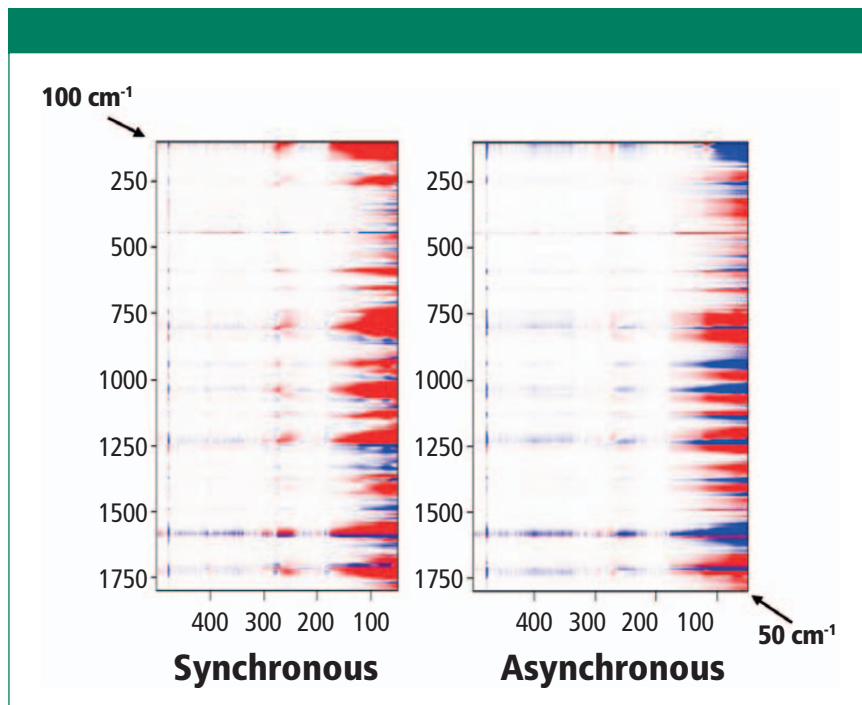


Figure 10: Synchronous (left) versus asynchronous (right) 2D COS in the heteroregion, crossing the full spectrum with the low-frequency behavior.

on one axis and then 1550 and 1800 cm^{-1} on the other axis because these spectra indicate how changes

in the conformation of the glycol are related to the changes in the carbonyl region. Then Figure 10 shows

slices of the 2D COS plots with almost the full spectrum along y (100 to 1800 cm^{-1}) and the low frequency region along x (50 to 500 cm^{-1}). Having normalized all spectra to the peak intensity of the aromatic band at 1614 cm^{-1} (the most constant feature in the spectrum) we can look at the spectra and say, for example, that the 1120 cm^{-1} band does not change very much but the 1096 cm^{-1} band grows as the material is converted to the trans conformation as the temperature is raised above T_g . In fact, the asynchronous plot does show these bands changing sequentially.

To see this change more clearly, first look at Figure 7, which shows the 2D COS plots in the region of the glycol bands. On the synchronous plot on the left we can see clearly the gain in intensity (red color) of the band at 1096 cm^{-1} but the increase in intensity of the band at 1000 cm^{-1} is less clear. That only really shows up in Figure 7b where the region around 1000 cm^{-1} is expanded. Now, when examining the horizontal axis close to 1000 cm^{-1} we can see a faint blue area centered at $x = 1030 \text{ cm}^{-1}$, which is the band that is replaced by the 1000 cm^{-1} band in the oriented or crystalline form. In the asynchronous plot we confirm that the band near 1000 cm^{-1} appears after the band at 1030 cm^{-1} .

In Figure 8, we can examine the carbonyl region in the same way. In the synchronous plot we can see the strong increase in the band at 1725 cm^{-1} that is known to increase in the crystal form. In addition, we see that the band near 1720 cm^{-1} is much less affected than the band at 1725 cm^{-1} . The band near 1735 cm^{-1} is curiously increasing with the 1725 cm^{-1} band. We can start to suggest assignments to the components in the carbonyl region. Note that there are two carbonyl groups on each aromatic group that presumably can interact. In the crystalline form, when they move in sync the mode will be Raman active, but when they move out of phase, the motion will be infrared (IR) active only. But in the amorphous material, there is no

center of symmetry so the selection rule is no longer valid. Presumably both modes of motion will be active in the Raman spectrum—accounting for the two broad bands near 1720 and 1735 cm^{-1} , and my guess is that the band at 1720 cm^{-1} would be the asymmetric (more IR active) mode, which is consistent to the assignment of the overtone of the carbonyl band in the IR spectrum at 3433 cm^{-1} (15).

Now we want to look at the relationships between the bands of the glycol group and the carbonyl. Figure 9 shows the 2D COS map for 700 to 1200 cm^{-1} along y (glycol bands) and 1550 to 1800 cm^{-1} along x (aromatic and carbonyl bands). Let's look at the y -axis at 1725 cm^{-1} . There are positive bands just under 1000 cm^{-1} , and at 1096 cm^{-1} . However, there are negative bands centered at about 875, 1030, and 1120 cm^{-1} . These are bands that we know have decreased intensity in the "crystalline" form when the 1725 cm^{-1} carbonyl band grows. There are also two lobes between

1175 and 1200 cm^{-1} that represent a band shift in the crystalline form, something that we haven't focused on in this discussion. But clearly one is going up as the other is going down—an observation consistent with some of the amorphous material being consumed by the crystalline transformation. Note that the vertical axis just above 1600 cm^{-1} also confirms the presence of a second band in the aromatic region that we had to consistently use in the band fitting; the two components clearly separate even though the lower energy part only appeared as an asymmetry in the spectral traces.

Finally, we look at the relationship between the low-frequency spectrum and the fingerprint or aromatic-carbonyl region that is shown in Figure 10. Actually, looking for the relationship between a low-frequency crystalline band (such as the rotation at 78 cm^{-1}) and the higher-frequency vibrations is not so straightforward. Perhaps one can examine the bands

representing combinations of C-C and C-O stretches (700–1150 cm^{-1}) in comparison to the low-frequency twists, but in discussing these results with Professor Noda, we realized that there was a problem with the experimental design for the low-frequency data. Because the spectral intensity is modulated by the Bose factor (which is a function of the spectral shift and the temperature), and that factor will be quite important in the low-frequency region, any comparison of low-frequency spectra recorded at different temperatures will have significant systematic errors. So, to achieve our goal of determining the relationship between atomic motions and crystallinity, we now realize that we have to make a different set of measurements. The next set of measurements will be an isothermal crystallization because under these conditions the Bose factor will not change from spectrum to spectrum. Stay tuned for a future installment on this topic.

ONDAX

RAMAN SPECTROSCOPY PRODUCTS

See what you've been missing with THz-Raman®

Structural Fingerprint

Both Stokes and anti-Stokes signals down to 5 cm^{-1}

Chemical Fingerprint

Complete chemical fingerprint

THz-Raman

High Throughput Screening

Ultra-low Frequency THz-Raman® Systems & Notch Filters

Microscope and Benchtop

In-situ Process Probes

Transmission Mode for Bulk Testing

SureLock **CleanLine** **Specializing in low-frequency Raman Systems and Components**

Wavelength Stabilized and Single Frequency Lasers from 405nm to 1064nm

ONDAX Online Store

Advanced Solutions for Optical Measurements

850 E. Duarte Rd. Monrovia, CA 91016
T. 626.357.9600 (Tel) | F. 626.513.7494 | sales@ondax.com

© 2018 Ondax, Inc.

Discussion

The novice studying polymer behavior can be overwhelmed by the concepts and nomenclature that are presented. A polymer can be “crystalline,” but the nature of the crystallinity will be different than for other solids based on smaller molecular species. The point to be recognized is that because the length dimension of the chain is so much larger than its lateral dimensions there is the certainty that there will be chain “entanglements.” Presumably, these chain entanglements are what affects the limitations preventing 100% crystallization. Once the chains are entangled, it is highly unlikely that they will magically untangle and align. Models of partially crystalline polymers describe regions where the chains do line up, but there may be limited lengths of a given chain that will reside in crystalline regions, while the rest of the same chain will be in amorphous regions. Then if the material is “drawn,” which means stretched out, parts of chains can likewise be lined up, and the entangled parts will remain in amorphous disordered regions. What we found many years ago (16) in our PET fibers that had been drawn at room temperature was that they aligned, without crystallizing because the treatment was done well below T_g (~90 °C). And we also found that the fiber that originally had the least amount of orientation and crystallinity from manufacture was the one that could be drawn and oriented the most.

Because of the structural use of polymers, it is important to understand the origin of their strength, elongation to break, elasticity, flexibility, and so on. Clearly, only knowing the amount of crystalline versus amorphous material will not tell the entire story. And that is where spectroscopy can help. Unlike XRD which can only characterize the crystalline phase, spectroscopy has the capability to analyze the amorphous phase as well, including its degree of orientation and the conformation of some important functional groups. Note that it will not be possible to orient entangled material, but the entangled

material may increase strength against breakage. By drawing the molecular chains, the material is predisposed to crystallization. Thus, it becomes clear why spectroscopy, in combination with other physical measurements, can be critical in predicting a material's behavior, based on its history.

So, I haven't yet gotten the result that I am after—that is, to determine details of the crystallization process in polyethylene terephthalate. Stay tuned. This determination will require another set of measurements. My apologies to the purists of my readers who feel that an unfinished project is not worthy of publication. Remember that my goal here is to indicate what this technology can offer, so showing the entire process in painful detail may be helpful to some.

Acknowledgment

My sincerest thanks to Professor Isao Noda for encouraging me in this work and making extremely useful critical comments. I should also indicate how sad I am that Herman Noether, with whom I originally worked on these polymers, is no longer with us to see how useful this technology can be to his polymer physics.

References

- (1) F.J. Deblase, M.L. McKelvy, M. Lewin, and B.J. Bulkin, *J. Polym. Sci Polym. Lett. Ed.* **23**, 109–115 (1985).
- (2) R. deDaubeny, C.W. Bunn, and C.J. Brown, *Proc. Roy. Soc. A.* **226**, 1167 (1954).
- (3) D.I. Bower and W.F. Maddams, in the *Cambridge Solid State Science Series*, E.A. Davis and I.M. Ward, Eds. (Cambridge U. Press, UK, 1992).
- (4) A.J. Melveger, *J. Polym. Sci. A.* **10**, 317–322 (1972).
- (5) T. Achibat, A. Boukenter, E. Duval, G. Lorentz, and S. Etienne, *J. Chem. Phys.* **95**(4), 2949–2954 (1991).
- (6) F.J. Boerio, S.K. Bahl, and G.E. McGraw, *J. Polym. Sci., Polym. Phys.* **14**, 1029–1046 (1976)
- (7) F. Adar, D. Armellino, and H. Noether, “Raman Microprobe Spectroscopy of Polyethylene Terephthalate Fibers: Separation by Band-Fitting of Amorphous-Oriented and Crystalline

Components,” *SPIE 1336 Raman and Luminescence Spectroscopies in Technology II*, 182–193 (1990).

- (8) K. Schmidt-Rohr, W. Hu, and Z. Zumbulyadis, *Science* **280**, 714–717 (1998).
- (9) F. Adar and H. Noether, “Use of Band-Fitted Raman Spectra for the Characterization of Polymers and Measurement of the Oriented Amorphous Phase,” *SPIE 1636 Applied Spectroscopy in Materials Science* (1992).
- (10) J.C. Rodriguez-Cabello, L. Quintanilla, and J.M. Pastor, *J. Raman Spectroscopy* **25**, 335–344 (1994).
- (11) C.C.C. Lesko, J.F. Rabolt, R.M. Ikeda, B. Chase, and A. Kennedy, *J. Molecular Structure* **521**, 127–136 (2000)
- (12) S. Yang and S. Michielsen, *Macromolecules* **35**(27), 10108–10113 (2002).
- (13) M. Richard-Lacroix and C. Pellerin, *Macromolecules* **45**, 1946–1953 (2012).
- (14) 2DShige, developed by Prof. Shigeaki Morita (Osaka Electro-Communication University, Japan). Available at: <https://sites.google.com/site/shigemorita/home/2dshige>.
- (15) G. Dandilooti, G.K. Govaris, and V.G. Gregoriou, *Appl. Spec.* **58**(9), 1082–1092 (2004).
- (16) F. Adar and H. Noether, “Use of Band-Fitted Raman Spectra for the Physical Characterization of Polymers and Measurement of the Oriented Amorphous Phase,” *SPIE 1636 Applied Spectroscopy in Materials Science II*, 42–52 (1992).



Fran Adar is the Principal Raman Applications Scientist for Horiba Scientific in Edison, New Jersey. Direct correspondence to: SpectroscopyEdit @UBM.com

For more information on this topic, please visit:
www.spectroscopyonline.com



Determination of the Bulk Elemental Composition of Cast Iron with Glow Discharge Optical Emission Spectrometry (GD-OES)

Allen Metz and Aaron Walczewski, LECO Corporation

Cast irons are a family of ferrous alloys containing percent levels of carbon and silicon. Alloying elements such as chromium and nickel enhance the physical properties of the metal while the structure maintains a rich carbon phase. Whether the objective is to improve the strength, abrasion resistance, corrosion resistance, or hardness of the basic iron, the chemical composition must be controlled in order to achieve the desired physical properties.

Glow discharge spectrometry (GD-OES) is an analytical method for direct determination of the elemental composition of solid samples like cast iron. Through a process called cathodic sputtering, kinetic energy is transferred from the inert gas ions to the atoms on the sample surface, which causes some of these surface atoms to be ejected into the plasma. Once the atoms are ejected into the plasma, they are subject to inelastic collisions with energetic electrons or metastable argon atoms. Energy transferred by such collisions causes the sputtered atoms to become excited. The excited atoms quickly relax to a lower energy state by emitting photons. A spectrometer is used to measure the emission signals from the glow discharge. Since the number of photons emitted by each element is proportional to its relative concentration in the sample, analyte concentrations can be deduced by calibration with reference samples of known composition.

Results

$n = 5$ BS 286AC - Nodular Cast Iron										
Element	C	Si	Ni	Cr	V	Mo	Cu	Mg	Ti	B
Average	3.23	2.06	1.350	0.166	0.153	0.247	0.336	0.039	0.049	0.0083
Certified	3.24	2.03	1.360	0.165	0.151	0.258	0.341	0.034	0.054	0.0085
% Diff	-0.3%	1.5%	-0.7%	0.6%	1.3%	-4.5%	-1.5%	12.8%	-10.2%	-2.7%
Stdev	0.01	0.009	0.004	0.0003	0.0003	0.001	0.001	0.001	0.0003	0.0001
RSD	0.45	0.44	0.32	0.21	0.21	0.41	0.31	2.7	0.62	1.3

$n = 5$ BS 291DE - Chill Cast Iron													
Element	C	Si	Ni	Cr	V	Mo	Cu	Mg	Ti	Al	Nb	Co	B
Average	3.35	2.34	0.17	0.159	0.015	0.0201	0.192	0.047	0.0244	0.0065	0.0024	0.0082	0.0083
Certified	3.35	2.32	0.17	0.159	0.013	0.0220	0.189	0.040	0.0265	0.0089	0.0024	0.0062	0.0089
% Diff	0.0%	0.9%	2.3%	0.0%	10.3%	-9.5%	1.6%	14.2%	-8.6%	-36.5%	0.0%	24.7%	-7.2%
Stdev	0.02	0.008	0.002	0.001	0.0006	0.0005	0.0009	0.0007	0.0004	0.00009	0.0004	0.0006	0.00006
RSD	0.48	0.35	1.2	0.48	4.4	2.5	0.48	1.6	1.7	1.4	16.1	7.3	0.78

$n = 5$ Common Brake Rotor												
Element	C	Si	Ni	Cr	V	Mo	Cu	Mg	Ti	Al	Nb	Co
Average	3.74	1.87	0.063	0.140	0.0069	0.060	0.228	0.0052	0.0085	0.0031	0.0042	0.0132
Stdev	0.01	0.01	0.001	0.005	0.0004	0.004	0.004	0.0003	0.0006	0.0001	0.0005	0.0003
RSD	0.36	0.73	1.6	3.6	5.7	7.2	1.8	5.6	7.2	3.3	11.5	2.5

Spectrometer

LECO GDS900-RC

Experimental Conditions

Lamp: Grimm-style DC 4 mm

Voltage: 1250 V

Current: 45 mA

Conclusion

GD-AES was used to measure the bulk elemental composition of three cast iron samples with exceptional accuracy and precision. Even real world samples, with less homogeneity than certified reference materials, return consistent results. The glow discharge technique is more than capable to meet the analytical requirements of foundries and metals processing firms.

Reference

- (1) K.A. Marshall, *J. Anal. At. Spectrom.* **14**, 923–928 (1999).

LECO Corporation

3000 Lakeview Avenue, St. Joseph, MI 49085

tel. (269) 985-5496, fax (269) 982-8977

Website: www.leco.com



Chemometrics in Spectroscopy

Calibration Transfer Chemometrics, Part II: A Review of the Subject

We continue with our review of the methods and mathematics involved with the subject of calibration transfer. Calibration transfer involves several strategies and mathematical techniques for applying a single calibration database consisting of samples, reference data, and calibration equations to two or more instruments. In this installment, we continue by providing a review of the chemometric and tactical strategies used for the calibration transfer process.

Jerome Workman Jr. and Howard Mark

The basic methods that have been published related to calibration transfer mathematics and the techniques involved in this process are discussed as a continuation of our previous column (1).

Successive Projections Algorithm

The use of the successive projections algorithm (VSPA) to select variables for building robust transferable multiple linear regression (MLR) models has been demonstrated (2). Robust MLR models have been compared to partial least squares (PLS) models using piecewise direct standardization (PDS) to correct the secondary or child instrument spectra. In data sets tested, the mean prediction errors at the child instrument for the robust VSPA-MLR and the PLS-PDS models were comparable, and slightly better for VSPA-MLR. The VSPA approach appears to be a valid alternative to the commonly used PLS-PDS technique.

An example of the VSPA for selecting variables for building robust transferable MLR models has also been demonstrated. The transfer sample set is selected using a Kennard–Stone (KS) algorithm or modified VSPA that is applied on the rows of the instrument response matrix.

In published examples, the mean prediction errors of the secondary or child instrument are similar for VSPA-MLR as compared to PLS-PDS models. For some applications, the VSPA-MLR method produces lower prediction errors.

Compressed Wavelet Domain

Direct standardization in the compressed wavelet domain is termed *WTDS*. Calibration transfer in the compressed wavelet domain permits a reduction in processing time for the analysis of large spectral data sets with some success in calibration transfer (3).

In a published example, wavelet transform methods such as denoising, compression, and multiscale analysis have been developed for near-infrared (NIR) calibration transfer. Combined methods have been empirically tested to improve the precision of PDS. Methods compared have included

- wavelet denoising and piecewise direct standardization (WDPDS);
- wavelet compression and piecewise direct standardization (WCPDS); and
- wavelet multiscale and piecewise direct standardization (WMPDS).

Optimal results have been reported for these combined methods on various data (4).

Canonical Correlation Analysis

A method based on canonical correlation analysis (CCA) for calibration model transfer was developed for calibration transfer (5). In this work, two real NIR data sets were tested in a comparative study between CCA and PDS. A comparison of methods was most positive for the CCA technique.

Positive Matrix Factorization

Another approach to calibration transfer has been developed based on a revised factorization technique called *positive matrix factorization* (PMF). PMF was developed and initially applied to environment data analysis (6). It has important differences from PCA. Because it is a least squares approach to solving the factor analysis problem, it can use subjective weights for individual data points and thereby allows the inclusion of uncertain data points—for example, missing data or analysis values below the detection limit.

Spectral Regression

A calibration transfer method for NIR spectra based on spectral regression has been examined (7). A comparative study of a spectral method and PDS for standardization on two benchmark NIR data sets was demonstrated with the results using spectral regression similar to those obtained using PDS with background correction.

A procedure for the transfer of the regression equation in NIR spectroscopy, from a first (parent) instrument to a second (child) instrument, is presented in an example paper (8). The procedure uses PLS regression twice: in the first step to compute the relationship between the spectra of transfer samples of the two instruments, and in the second step to compute the regression equation (relationship between chemical variables and spectral variables) of the first instrument. In the example paper, spectra were recorded with four different instruments, in four different laboratories with transfer results given, and reported as standard error of prediction. The spectral regression method prediction results for the transfer instrument were reported to be comparable to the original calibration.

Wavelet Packet Transform Standardization

A standardization algorithm, called *wavelet packet transform standardization* (WPTS), based on a wavelet packet transform (WPT) and entropy criteria, was proposed to transfer spectra between two NIR spectrometers (9). By comparison, the example WPTS produces a predicted value transfer performance comparable to wavelet transform standardization 1 (WTS1), which is considered one of the best existing transfer methods, and better than wavelet transform standardization 2 (WTS2) combined with standard PDS (WTS2-PDS).

The WPTS method also has a low computational requirement as an added benefit.

Stacked Partial Least-Squares Regression

A paper demonstrated the use of stacked partial least-squares (SPLS) regression and stacked dual-domain (SDD) regression analysis combined with commonly used techniques for calibration transfer to improve predictive performance from transferred multivariate calibration models (10). The paper reported that the predictive performance for gasoline samples was improved when combined with three conventional calibration transfer methods—namely, PDS, orthogonal signal correction (OSC), and model updating (MUP). These methods require transfer standards to be measured on both instruments.

Multiplicative Scatter (or Signal) Correction

An applications paper compares two multiplicative signal correction (MSC) algorithms for the standardization of data from two NIR spectrometers (11). Absorbance spectra were measured in the 1000–2200 nm range for a set of 45 jet fuel samples. Data from one instrument were standardized to match data from a second instrument using windowed MSC (W-MSC) and moving window MSC (MW-MSC). For W-MSC user-defined windows were selected and for MW-MSC the window size was optimized based on a two-step proce-

The Spectroscopy Specialists

Pathlengths from 0.01mm to 100mm
Volumes from 0.6ul to 35ml
Far UV & NIR Quartz
Glass & Borosilicate



Starna

Starna Cells, Inc.

PO Box 1919 Atascadero, CA 93423

Phone: (800) 228-4482 USA or (805) 466-8855 outside USA
sales@starnacells.com www.starnacells.com

ture: assigning a cut off window to avoid over-processing and selection of a specific window size based on sample leverage.

Multiplicative scatter (or signal) correction provides some mitigation of the scattering phenomenon by regressing the individual spectrum to the mean spectrum of a collection of spectra, for both calibration and prediction datasets (12–15). The identical algorithm must be completed for both calibration and prediction sets. When conditions or datasets are changed the algorithm is recomputed for the entire set. The algorithm assumes that the ideal spectrum is the mean spectrum, which is an oversimplification, but it provides a basis for making some correction. Light scatter and spectral measurements are complex and poorly understood so correction algorithms, although useful, do not present an ideal theoretical correction for the scattering phenomenon, but only an approximation.

For the MSC algorithm, each spectrum in a set of spectra represents the dependent variable (as a vector) in a least squares regression case where the mean spectrum is the independent variable (also a vector). From this computation, both the slope and intercept MSC variables are computed. So, the general least squares formula in standard notation is as shown in equation 1:

$$a_i = o_i + b_i \bar{a}_i + e_i \quad [1]$$

For this least squares linear regression equation, a_i is an individual spectrum i from the dataset, \bar{a}_i is the mean spectrum of the set of spectra, o_i is the bias or offset, and e_i is the residual spectrum.

The estimated or corrected MSC spectrum is computed using the computed slope (b_i) and intercept (o_i) constants as shown in equation 2:

$$\hat{a}_i (MSC) = \frac{(a_i - o_i)}{b_i} \quad [2]$$

MSC approximates a regression

estimate of the mean spectrum with the remaining unexplained residual spectrum representing the spectral differences between the spectra within a set. This residual difference is assumed to contain much of the chemical information differences between samples in the spectrum set.

Standard Normal Variate

The standard normal variate (SNV) data preprocessing method partially compensates for some spectral slope and particle size differences within a series of spectra measured using diffuse reflection (16–19). The algorithm is applied individually to each spectrum for both calibration and prediction spectra. This processing step is applied to each data point for each spectrum using the mean and standard deviation of the spectrum in absorbance space (units). The computation is straightforward as the mean absorbance difference for each data point to the mean absorbance of the spectrum ratioed to the standard deviation of the absorbance for the spectrum. The computation formula is as shown in equation 3:

$$a_{ij} (SNV) = \frac{(a_{ij} - \bar{a}_i)}{\sqrt{\frac{\sum_{i=1}^n (a_{ij} - \bar{a}_i)^2}{n-1}}} = \frac{\text{mean.difference}}{\text{standard.deviation}} \quad [3]$$

where $a_{ij} (SNV)$ is the computed standard normal variate for the datapoint (element) a_{ij} , \bar{a}_i is the mean of the spectrum i , and n is the number of data points or elements in the spectrum.

Detrend

Detrend is a general term used to describe the removal of a basic trend from data to more closely determine the signal attributes associated with analyte concentration or basic information content in a signal (16). To remove the trend (that is, detrend) data in a time series a linear least squares fit is determined for the data and then subtracted from the data. For unusual shapes, such as spectra,

a polynomial function of a selected order is fit to all the data points in the spectrum and subtracted from the spectrum. The polynomial is used to fit all data points in the spectrum. This technique will remove large background interference, or specific trending variation, and is often used in combination with the SNV preprocessing function. A detrend algorithm consists of a polynomial or linear fit to each spectrum and a subtraction function of the fit function from the spectrum.

Classification Methods

Spectrometer instruments are characterized by classifying their spectra into previously defined clusters. The spectra are mapped to the clusters and a classification is made based on the similarity of extracted spectral features to one of the previously defined clusters. Calibration models for each cluster are provided to compensate for within or between instrumental variation. A simplified method of calibration transfer maps clusters to each other, so that a calibration transferred between clusters models only the difference between the two clusters, substantially reducing the complexity of the models used for transfer (20).

Synthetic Calibration Spectra

A spectrum simulation method is described for use in the development and transfer of multivariate calibration models from NIR spectra (21). By use of previously measured molar absorptivities and solvent displacement factors, synthetic calibration spectra are computed using only background spectra collected with the spectrometer for which a calibration model is desired. The resulting synthetic calibration set is used with PLS regression to form the calibration model. This methodology is demonstrated for use in the analysis of physiological levels of glucose (1–30 mM) in an aqueous matrix containing variable levels of alanine, ascorbate, lactate, urea, and triacetin.

Dispersive to Fourier Transform Transfer

NIR calibration models have been developed for the determination of content uniformity in pharmaceutical tablets (22). Data used in one study were acquired from five NIR instruments manufactured by two different vendors. One of these spectrometers was a dispersive-based NIR system while the other four were Fourier transform (FT) based. The transferability of the optimized PLS calibration models developed on the primary instrument (A) located in a research facility was evaluated using spectral data acquired from secondary instruments B, C, D, and E. Instruments B and E were located in the same research facility as spectrometer A while instruments C and D were located in a production facility 35 miles away. The same set of tablet samples was used to acquire spectral data from all instruments. To minimize the effect of instrument variability, calibration transfer techniques such as PDS and wavelet hybrid direct standardization (WHDS) were used.

A principal component regression calibration model developed on a scanning NIR spectrophotometer (with a standard cuvette) was transferred to a Fourier transform NIR spectrophotometer (with a fiber-optic probe) for the determination of sodium chloride in aqueous solutions by using the piecewise direct standardization method (23). Only two transfer samples were needed in obtaining a good calibration transfer.

Dispersive to Handheld Transfer

The objective of one study was to assess the potential of calibration transfer from the Foss NIRSystem 6500 instrument to the Polychromix Phazir instrument (24). The results show that good calibration models were obtained for various feed properties (that is, fat, fiber, protein, and starch) developed on a Foss NIRSystem 6500 instrument, based on a spectral database of 9164 samples transferred to a microelectromechanical (MEMS)-based Polychromix Phazir handheld spectrometer.

Temperature Compensation

Calibration transfer between spectra measured at different temperatures was investigated for NIR spectroscopic determination of sodium chloride in aqueous solutions (25). A PCR calibration model developed at 23.0 °C was transferred to a model at 28.5 °C by using a PDS method.

Two-Dimensional Method Transfer

A method for calibrating two-dimensional (2D) responses measured on multiple instruments or on a single instrument under different operating conditions has been demonstrated (26). From computer simulation and experimental data, it was found that the design of the standard sample spectral profile is crucial for the parameter estimations and response standardization. This is because of the phenomenon that instrument response is ample dependent.

Compensating for Extraneous Phenomena (or Unmodeled Variation)

The analysis accuracy and precision of any multivariate calibration method will be severely degraded if unmodeled sources of spectral variation are present in the unknown sample spectra. A synthetic generalized method was developed and published for correcting errors generated by the presence of unmodeled components or spectral variation (27). This method requires that the spectrum of the unmodeled component be simulated or measured and mathematically added in variable amounts to the original calibration spectra. After this adjustment, a revised calibration model is generated. This new calibration accommodates the unmodeled source of spectral variation. This method minimizes the effect of long-term drift on prediction errors and using the synthetic method eliminates the need for the expensive generation of new calibration samples.

The method is referred to as *prediction-augmented classical least-squares (PACLS)*, and does not require that all interfering spectral characteristics be known during the calibration process. PACLS can correct calibration models if unmodeled spectral components can be identified, simulated, and added during a PACLS prediction step (28). The addition of a classical least-squares–partial least-squares (CLS–PLS) hybrid algorithm, and a prediction-augmented classical least-squares–partial least-squares (PACLS–PLS) hybrid algorithm improves the cal-

EDINBURGH INSTRUMENTS

GLOBAL LEADERS

IN

FLUORESCENCE SPECTROSCOPY

SINCE 1971

Edinburgh Instruments have been at the
forefront of research, development and state
of the art photoluminescence instrumentation
for over 40 years.

Proudly made in the UK.



EDINBURGH
INSTRUMENTS

www.edinst.com
+44 (0)11 556 425 300
info@edinst.com

Edinburgh Instruments
2 Bann Square
Kirkton Campus
Livingston
EH54 7DD
United Kingdom

ibration process even in the presence of unmodeled sources of spectral variation (29,30).

An additional prediction-augmented classical least-squares-partial least-squares (PACLS-PLS) hybrid algorithm has been demonstrated for use in calibration transfer between instruments (31). Dramatic spectral differences caused by deviations in instrument response are incorporated into the algorithm through the use of sample spectra measured on both parent and child spectrometers.

Creating Transferable Calibrations in Mid-IR

Sensitivity studies showed that detector nonlinearity, frequency accuracy, incident angle, and variation in purge gases are important parameters to obtain transferable calibrations for Fourier transform infrared (FT-IR) calibrations (32). As the complexity of the modeled variables and calibration increases, calibration transfer becomes more challenging. Outlier detection methods are useful to determine instrument similarity and goodness of fit for a specific spectrum to a calibration database. Calibrations that maintained limited variance in instrument factors, subtracted purge gas spectra, and used data from specific robust frequencies were successfully transferred, and were also robust against spectrometer drift.

Summary

This column completes the overview of calibration transfer mathematical approaches. As new techniques are developed and published we hope to provide updates on this topic.

References

- (1) J. Workman Jr. and H. Mark, *Spectroscopy* **32**(10), 18–24 (2017).
- (2) F.A. Honorato, R.K.H. Galvão, M.F. Pimentel, B. de Barros Neto, M.C.U. Araújo, and F.R. de Carvalho, *Chemom. Intell. Lab. Syst.* **76**(1), 65–72 (2005).
- (3) J. Yoon, B. Lee, and C. Han, *Chemom. Intell. Lab. Syst.* **64**(1), 1–14 (2002).
- (4) J.X. Wang, Z.N. Xing, and J. Qu, *Spectroscopy* **28**(6), 36–41 (2013).

- (5) W. Fan, Y. Liang, D. Yuan, and J. Wang, *Anal. Chim. Acta* **623**(1), 22–29 (2008).
- (6) Y. Xie and P.K. Hopke, *Anal. Chim. Acta* **384**(2), 193–205 (1999).
- (7) J. Peng, S. Peng, A. Jiang, and J. Tan, *Spectrochim. Acta, Part A* **78**(4), 1315–1320 (2011).
- (8) M. Forina, G. Drava, C. Armanino, R. Boggia, S. Lanteri, R. Leardi, and R. Bigoni, *Chemom. Intell. Lab. Syst.* **27**(2), 189–203 (1995).
- (9) T.A.N. Chao and L.I. Menglong, *Anal. Sci.* **23**(2), 201–206 (2007).
- (10) W. Ni, S.D. Brown, and R. Man, *Anal. Chim. Acta* **661**(2), 133–142 (2010).
- (11) K.E. Kramer, R.E. Morris, and S.L. Rose-Pehrsson, *Chemom. Intell. Lab. Syst.* **92**(1), 33–43 (2008).
- (12) P. Geladi and E. Dåbakk, *J. Near-Infrared Spectrosc.* **3**(3), 119–132 (1995).
- (13) M.S. Dhanoa, S.J. Lister, R. Sanderson, and R.J. Barnes, *J. Near-Infrared Spectrosc.* **2**(1), 43–47 (1994).
- (14) H. Martens, J.P. Nielsen, and S.B. Engelsen, *Anal. Chem.* **75**(3), 394–404 (2003).
- (15) J.-W. Jin, Z.-P. Chen, L.-M. Li, R. Steponavicius, S.N. Thennadil, J. Yang, and R.-Q. Yu, *Anal. Chem.* **84**(1), 320–326 (2012).
- (16) R.J. Barnes, M.S. Dhanoa, and S.J. Lister, *Appl. Spectrosc.* **43**(5), 772–777 (1989).
- (17) A. Candolfi, R. De Maesschalck, D. Jouan-Rimbaud, P.A. Hailey, and D.L. Massart, *J. Pharm. Biomed. Anal.* **21**(1), 115–132 (1999b).
- (18) T. Woodcock, G. Downey, D. Kelly, and C. O'Donnell, *J. Agric. Food Chem.* **55**(22), 9128–9134 (2007).
- (19) K. Tanaka, Y. Kuba, T. Sasaki, F. Hiwatashi, and K. Komatsu, *J. Agric. Food Chem.* **56**(19), 8787–8792 (2008).
- (20) K.H. Hazen, T.B. Blank, S. Monfre, and T.L. Ruchti, "Method of Characterizing Spectrometer Instruments and Providing Calibration Models to Compensate for Instrument Variation," U.S. Patent 6864978 (2005).
- (21) Y. Sulub and G.W. Small, *Appl. Spectrosc.* **61**(4), 406–413 (2007).
- (22) Y. Sulub, R. LoBrutto, R. Vivilecchia, and B.W. Wabuyele, *Anal. Chim. Acta* **611**(2), 143–150 (2008).
- (23) J. Lin, S.C. Lo, and C.W. Brown, *Anal. Chim. Acta* **349**(1–3), 263–269 (1997).
- (24) J.A.F. Pierna, P. Vermeulen, B. Lecler, V. Baeten, and P. Dardenne, *Appl. Spectrosc.* **64**(6), 644–648 (2010).
- (25) J. Lin, *Appl. Spectrosc.* **52**(12), 1591–1596 (1998).
- (26) B.R. Kowalski and Y. Wang, "Calibration transfer for second order analytical instruments," U.S. Patent 5559728 (1996).
- (27) D.M. Haaland, *Appl. Spectrosc.* **54**(2), 246–254 (2000).
- (28) D.M. Haaland and D.K. Melgaard, *Appl. Spectrosc.* **54**(9), 1303–1312 (2000).
- (29) D.M. Haaland and D.K. Melgaard, *Appl. Spectrosc.* **55**(1), 1–8 (2001).
- (30) C.M. Wehlburg, D.M. Haaland, D.K. Melgaard, and L.E. Martin, *Appl. Spectrosc.* **56**(5), 605–614 (2002).
- (31) C.M. Wehlburg, D.M. Haaland, and D.K. Melgaard, *Appl. Spectrosc.* **56**(7), 877–886 (2002).
- (32) I.S. Adhietty, J.A. McGuire, B. Wangmaneerat, T.M. Niemczyk, and D.M. Haaland, *Anal. Chem.* **63**(20), 2329–2338 (1991).



Jerome Workman Jr. serves on the Editorial Advisory Board of *Spectroscopy* and is the Executive Vice President of Engineering at Unity Scientific, LLC, in Milford,

Massachusetts. He is also an adjunct professor at U.S. National University in La Jolla, California, and Liberty University in Lynchburg, Virginia.



Howard Mark serves on the Editorial Advisory Board of *Spectroscopy* and runs a consulting service, Mark Electronics, in Suffern, New York. Direct correspondence to: SpectroscopyEdit@UBM.com

For more information on this topic, please visit:
www.spectroscopyonline.com

Exploring the Applicability of Quantitative Models Based on NIR Reflectance Spectroscopy of Plant Samples

The establishment of quantitative models based on the near-infrared (NIR) spectroscopic analysis of plant samples plays an important role in improving both the scope of the models and the accuracy of prediction. In this study, four types of tobacco samples and their mixed products were selected as research objects. Based on the modeling methods of the different types of tobacco, this technique could provide a new method for tobacco quality management as well as provide a new discriminant method for other agricultural products.

Yuqing Yang, Li Ma, Guorong Du, Junhui Li, and Yanjun Ma

To improve the scope of models and the accuracy of their prediction, the establishment of quantitative models for different types of plants plays an important role. The quality characteristics of common food and cash crops, including wheat, rice, corn, tea, and tobacco, among others, differ because of genetic differences. Among these crops, tobacco exhibits typical characteristics of plants and can be divided into several types, including flue-cured tobacco, burley tobacco, dark sun-cured tobacco, and oriental and aromatic tobacco. Moreover, total nitrogen and total alkaloid contents are two important indicators of quality evaluation in tobacco and its products. The total nitrogen content is determined by the classical Kjeldahl method, and the total nicotine content is determined by continuous flow analysis (1,2). However, both methods are limited by the need for complex preprocessing, and the testing processes are time-consuming and can delay results; therefore, these methods do not meet the rapid detection and quality control needs of scientific research or the on-site quality acceptance of tobacco leaves. At present, local regression modeling and consensus modeling are used to analyze homogeneous plant samples that exhibit regional and temporal differences (3–7). Beyond ensuring the applicability of models, significantly improving their accuracy is difficult, so it

is important to develop a fast and accurate quantitative analysis method for improving the applicability of the models.

As a nondestructive and rapid analytical method, near-infrared (NIR) spectroscopy has been widely used for the qualitative analysis of various organic feedstocks and for physical and chemical quantitative analyses across the food, pharmaceutical, and agricultural industries (8,9).

A variety of chemical composition tests using quantitative NIR analysis have recently been carried out on flue-cured tobacco, burley tobacco, oriental and aromatic tobacco, and other types of tobacco (10–17). Previously, Tonini reported an NIR model of the total sugar content in both flue-cured tobacco and oriental and aromatic tobacco (18). The results were as follows: For flue-cured tobacco, the standard error of calibration (SEC) was 0.802 and the standard error of prediction (SEP) was 1.208; whereas for oriental and aromatic tobacco the SEC was 0.883, and the SEP was 0.976. These results showed that the single models were more accurate than were the hybrid models. Then, new pattern recognition methods by Zhang (19) using a partial least squares support vector machine (PLS-SVM) approach and by Shao (20) using wavelet transform combined with an artificial neural network (WT-ANN)

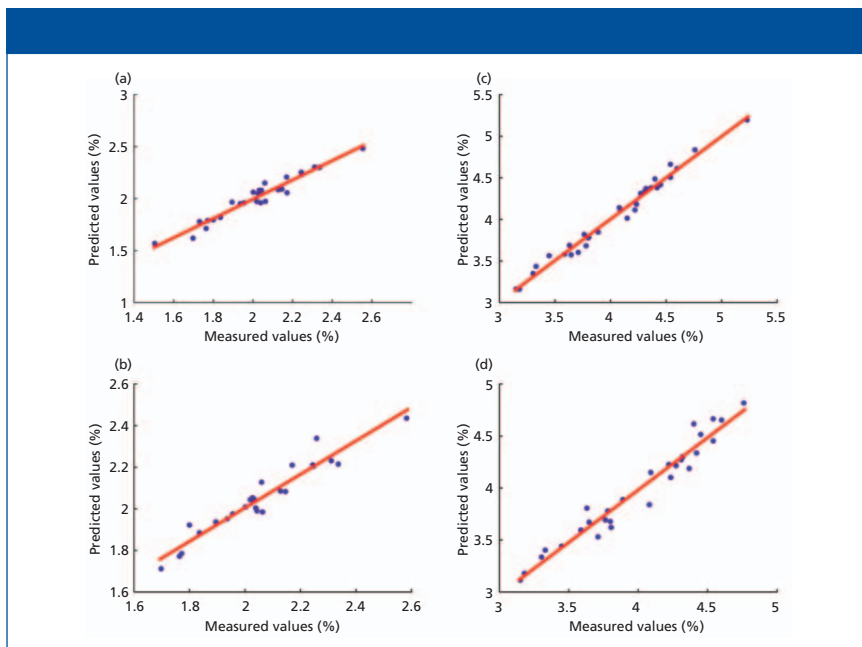


Figure 1: Comparison of single models predicting known samples and hybrid models predicting known samples of the total nitrogen of flue-cured tobacco and burley tobacco: (a) flue-cured tobacco and flue-cured tobacco, (b) burley tobacco and burley tobacco, (c) multitype tobacco and flue-cured tobacco, and (d) multitype tobacco and burley tobacco.

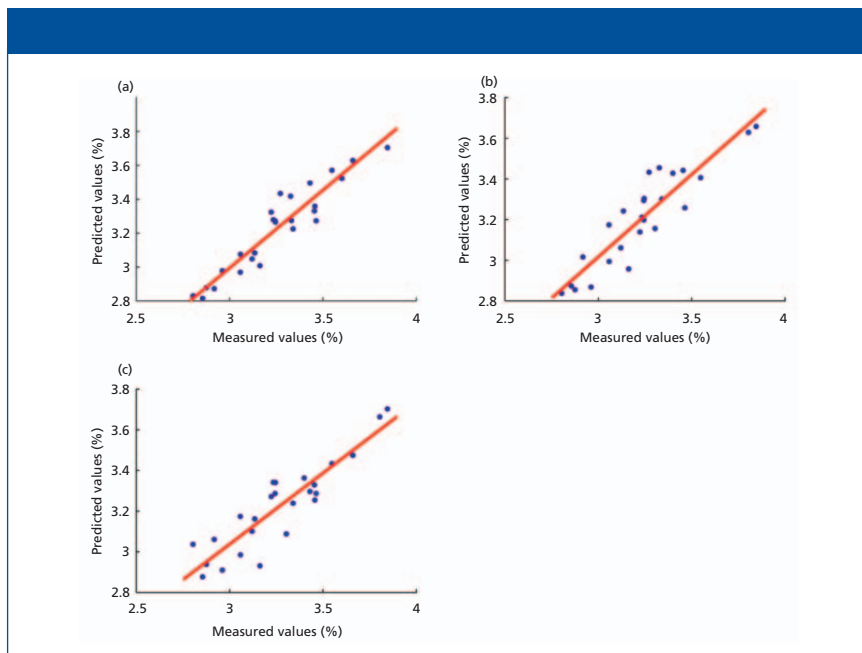


Figure 2: Comparison of single models predicting mixed samples and hybrid models predicting mixed samples of the total nitrogen of flue-cured tobacco and burley tobacco: (a) flue-cured tobacco and mixed tobacco, (b) burley tobacco and mixed tobacco, and (c) multitype tobacco and mixed tobacco.

were used to establish the quantitative and discrimination models and showed an excellent prediction performance for rapid and accurate analysis of routine chemical compositions in tobacco. To date, however, most studies essentially

report quantitative analysis methods of the main chemical constituents of flue-cured tobacco. The comparison of NIR single and hybrid models for total nitrogen and total alkaloid contents in other tobacco types has not been reported,

which strongly limits the applicability of quantitative models.

In this study, different types of tobacco were used as research samples. The total nitrogen content was determined by the Kjeldahl method, and the total alkaloid content was determined by continuous flow analysis. The spectra were determined by Fourier transform NIR spectroscopy and were preprocessed by the first derivative and smoothing methods. Single and hybrid quantitative analysis models for total nitrogen and total alkaloid contents in flue-cured tobacco, burley tobacco, dark sun-cured tobacco, oriental and aromatic tobacco, and mixed tobacco were ultimately established successively through the use of PLS and PLS-discriminant analysis (PLS-DA).

Materials and Methods

Materials

All the experimental samples of different tobacco types were collected at the Beijing Third Class Tobacco Supervision Station within a three-year period and are shown in Table I.

Spectral Measurements

A multipurpose analyzer with a near-infrared integrating sphere diffuse reflection accessory in reflectance mode (Bruker Optics Inc.) was used to measure spectra. In the experiments, wavenumbers ranging from 12,000 to 3500 cm^{-1} were measured at a digitization interval of approximately 8 cm^{-1} . The scan rate was 64 within 30 s, and all measurements were performed at room temperature. OPUS 7.0 quantitative analysis software (Bruker Optics Inc.) was used. The average of three normal spectra per sample was used.

Methods of Chemical Analysis

The total nitrogen in the tobacco samples was determined using a B-339 nitrogen analyzer (Buchi Labortechnik AG) in accordance with the Chinese tobacco industry YC/T 33-1996 standard. The total alkaloid content in the tobacco samples was determined using an AA3 continuous flow analyzer (Bran + Luebbe) in accordance with the Chinese tobacco industry YC/T 160-2002 standard. These data were used for subsequent modeling.

Analytical Methods

PLS was used to establish quantitative models of total nitrogen and total alkaloids for flue-cured tobacco, burley tobacco, dark sun-cured tobacco, oriental and aromatic tobacco, and mixed tobacco (21). Internal cross validation was used to determine the statistical parameters of the predictive NIR spectroscopy models. The calibration models were validated by verification sets. The SEP and mean of the SEP between the measured values and the predicted values of total nitrogen and total alkaloids were used as the evaluation parameters (22,23).

PLS-DA is a supervised pattern recognition method based on PLS and a combination of PLS regression and the discrimination analysis for classification tasks (24,25). The method uses a priori classification knowledge to establish a classification model using PLS-DA and then uses that model to discriminate the attributions of the samples to be tested.

Results and Discussion

Establishment of Single and Hybrid Models

For each type of tobacco, 150 samples were collected. Based on the distribution of total nitrogen and total alkaloid concentrations, 120 samples were selected for the modeling set, and the remaining samples (comprising 30 samples of mixed tobacco) were used for the validation set. Summaries of the statistical analysis results of the partially optimized PLS of the models of the different tobacco types for the total nitrogen and total alkaloid contents are shown in Tables II and III.

Both tables show that the R^2 of the quantitative NIR models of total nitrogen and total alkaloids among flue-cured tobacco, burley tobacco, dark sun-cured tobacco, oriental and aromatic tobacco, and multitype tobacco were greater than 0.90; the SEC values of the calibration sets were lower than 1; and the calibration models had better predictive ability.

Contrastive Verification of Models

The external prediction of the single and hybrid quantitative calibration models for total nitrogen and total alkaloids was carried out by using the 30 vali-

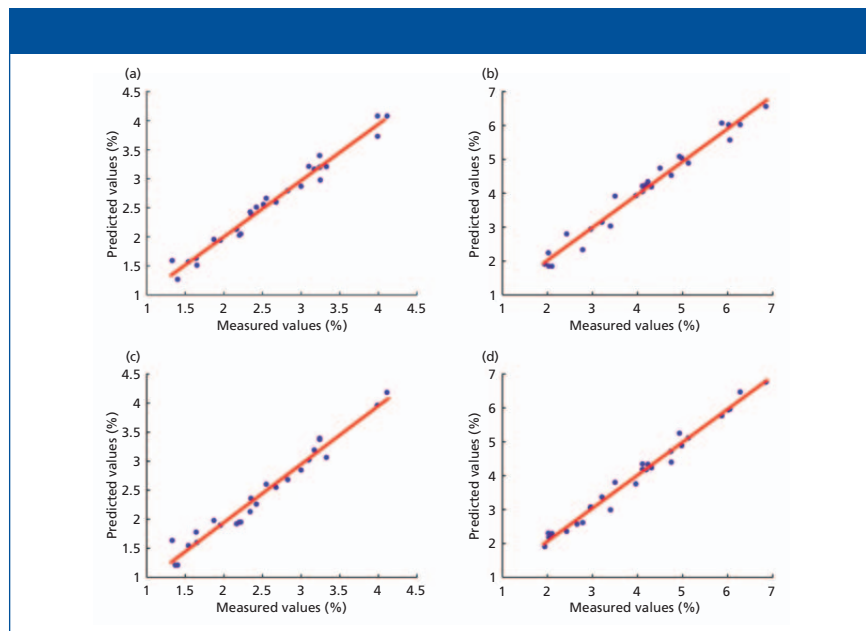


Figure 3: Comparison of single models predicting known samples and hybrid models predicting known samples of the total alkaloids of flue-cured tobacco and burley tobacco: (a) flue-cured tobacco and flue-cured tobacco, (b) burley tobacco and burley tobacco, (c) multitype tobacco and flue-cured tobacco, and (d) multitype tobacco and burley tobacco.

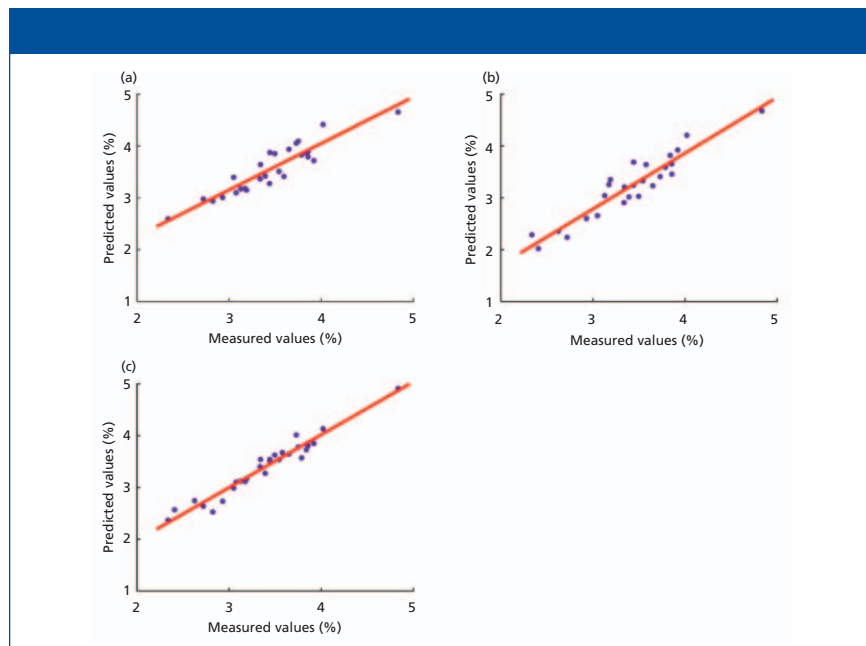


Figure 4: Comparison of single models predicting mixed samples and mixed models predicting mixed samples of the total alkaloids of flue-cured tobacco and burley tobacco: (a) flue-cured tobacco and mixed tobacco, (b) burley tobacco and mixed tobacco, and (c) multitype tobacco and mixed tobacco

dated samples. The predictive results of the different quantitative NIR analysis models for total nitrogen and total alkaloids are shown in Tables IV and V; the results are reported as SEP values. The prediction results of total nitrogen from the different models of tobacco are

shown in Tables VI and VII; the results are reported as the means of the SEP. Among these models, S-K, S-Mu, H-S, S-Mi, and H-Mi represent single models predicting known samples, single models predicting multitype samples, hybrid models predicting known samples, sin-

Types*	Composition	Numbers
Flue-cured tobacco	Flue-cured tobacco	150
Burley tobacco	Burley tobacco	150
Dark sun-cured tobacco	Dark sun-cured tobacco	150
Oriental and aromatic tobacco	Oriental and aromatic tobacco	150
Multitype tobacco	Flue-cured tobacco, burley tobacco, dark sun-cured tobacco, and oriental and aromatic tobacco	600
Mixed tobacco	Unknown types or mixed products	30

*The types of tobacco used in this experiment were essentially tobacco cultivars grown in China and represent a small portion of worldwide tobacco cultivars.

Parameter names	Flue-cured tobacco	Burley tobacco	Dark sun-cured tobacco	Oriental and aromatic tobacco	Multitype tobacco
Spectral range (cm ⁻¹)	8000–4000				
Preprocessing methods	First derivative				
Number of calibration sets	120	120	120	120	480
R ²	0.982	0.964	0.932	0.990	0.956
SEC	0.041	0.132	0.158	0.078	0.206
Prediction range (%)	0.88–3.36	1.87–5.55	2.44–5.42	1.56–5.55	0.88–5.55

Parameter names	Flue-cured tobacco	Burley tobacco	Dark sun-cured tobacco	Oriental and aromatic tobacco	Multitype tobacco
Spectral range (cm ⁻¹)	8000–4000				
Preprocessing methods	First derivative				
Number of calibration sets	120	120	120	120	480
R ²	0.963	0.971	0.946	0.983	0.981
SEC	0.134	0.237	0.326	0.124	0.248
Prediction range (%)	1.24–4.11	1.65–8.78	1.91–9.30	0.13–4.13	0.13–9.30

gle models predicting mixed samples, and hybrid models predicting mixed samples, respectively.

As shown in Tables IV and VI, in the forecast of the quantitative model of the total nitrogen content in the different types of tobacco (the data in the table are bold and italicized), the single models can predict known samples of total

nitrogen. The SEP values of flue-cured tobacco, burley tobacco, dark sun-cured tobacco, and oriental and aromatic tobacco were lower than those of the single models predicting multitype samples, demonstrating that the S-K models are better than the S-Mu models. Further, the error rate for predicting total nitrogen was reduced by 42.5% and for total

alkaloids by 63.8%, indicating that single models could predict only known samples but not mixed samples.

The comparison of the S-Mi and H-Mi models shows that the mean of the SEP was 0.210 for S-Mi, which was greater than that for H-Mi (0.185), so the accuracy of the single models predicting mixed samples was clearly weaker than that of the hybrid models. Compared with that of H-K, the error rate of H-Mi was reduced by 11.9% for total nitrogen and by 69.5% for total alkaloids. This finding indicates that the hybrid models are more suitable and broadly applicable; they can be used for the quantitative analysis of mixed products and are suitable for the quantitative analysis of other agricultural plants (for example, different varieties of corn and different modulation methods of tea). In particular, regarding the comparisons of H-K and S-K with S-Mu, for unknown types of tobacco, the H-K model can be applied, but its predictive effect is weaker than that of the S-K model but stronger than that the S-Mu model.

To verify the predictive effects, we further took flue-cured tobacco and burley tobacco as examples in this work and comparatively analyzed the total nitrogen and total alkaloids from the single model prediction of flue-cured tobacco (or burley tobacco) and hybrid model prediction of flue-cured tobacco (or burley tobacco) as well as from the single model prediction of mixed tobacco and hybrid model prediction of mixed tobacco. The correlations between the measured values and the predicted values of the verification sets are shown in Figures 1–4.

As shown in Figures 1–4, the total nitrogen and total alkaloids of the different tobacco types were concentrated on both sides of the line, and a high degree of analysis accuracy occurred with respect to the relationship between the measured values and the predicted values of the verification sets. Figures 1 and 3 show that the predictive effect of the single models is clearly better than that of the hybrid models. By contrast, Figures 2 and 4 show that the hybrid models constructed in this study have a wider predictive range for predicting mixed samples.

Table IV: Prediction results of the total nitrogen of the different types of tobacco–SEP values

Types	Flue-Cured Tobacco	Burley Tobacco	Dark Sun-Cured Tobacco	Oriental and Aromatic Tobacco	Multitype Tobacco	Mixed Tobacco
Flue-cured tobacco	0.066	0.358	0.318	0.276	0.232	0.144
Burley tobacco	0.259	0.194	0.34	0.332	0.223	0.362
Dark sun-cured tobacco	0.214	0.163	0.107	0.189	0.204	0.259
Oriental and aromatic tobacco	0.652	0.752	0.63	0.124	0.198	0.075
Multitype tobacco	0.062	0.127	0.199	0.173	0.134	0.185

Table V: Prediction results of the total alkaloids of the different types of tobacco–SEP values

Types	Flue-Cured Tobacco	Burley Tobacco	Dark Sun-Cured Tobacco	Oriental and Aromatic Tobacco	Multitype Tobacco	Mixed Tobacco
Flue-cured tobacco	0.127	0.565	0.643	0.685	0.870	0.218
Burley tobacco	0.833	0.237	0.623	0.699	0.587	0.281
Dark sun-cured tobacco	0.340	0.422	0.284	0.276	0.291	0.135
Oriental and aromatic tobacco	0.475	0.403	0.415	0.119	0.372	0.172
Multitype tobacco	0.160	0.266	0.341	0.175	0.191	0.125

Model Discriminant Analysis of Qualitative and Quantitative Combinations of Different Types of Tobacco

In practical applications, unknown sample types are often present. In general, one way of estimating sample types involves the use of hybrid models, and then, based on the predicted results and the empirically determined total nitrogen and total nicotine contents of the tobacco, samples suitable for classification are selected. To improve the accuracy of quantitative NIR analysis, the use of qualitative discrimination followed by a single quantitative analysis model can be employed.

PLS-DA, which is based on both qualitative and quantitative algorithms, can be used to determine the chemical composition of unknown samples. The PLS-DA was performed before the second derivative and smoothing (17) transformations, and cross validation was used to determine that the value of the factor was 10. The qualitative discriminant analyses between the different types of tobacco are shown in Figure 5, and the discriminant rates are shown in Table VIII.

Figure 5 shows that the qualitative identifications of the flue-cured tobacco were all correct, as were those of other sample types. Two of the burley tobacco types were incorrectly identified, but the

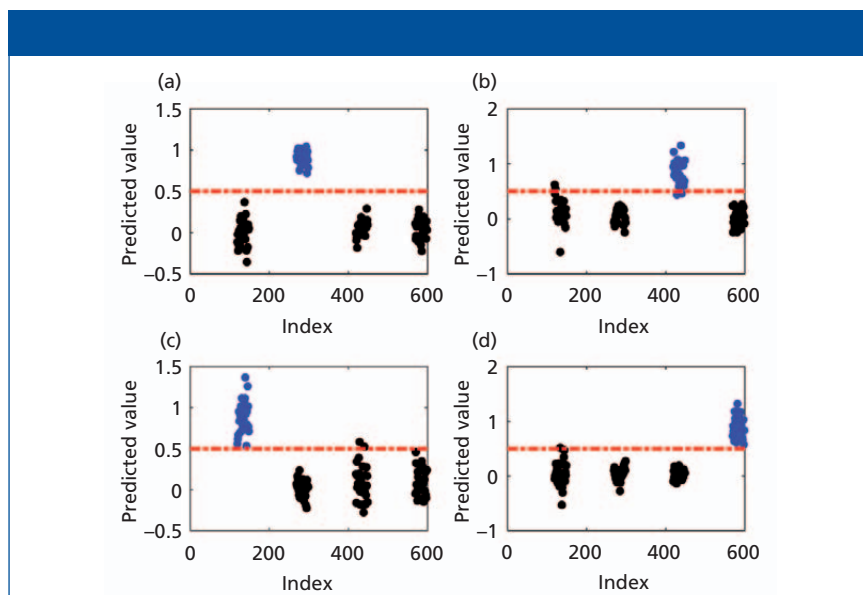


Figure 5: Prediction results based on PLS-DA of the various tobacco types: (a) flue-cured tobacco, (b) burley tobacco, (c) dark sun-cured tobacco, and (d) oriental tobacco.

others were correctly identified; two of the other sample types were mistaken as burley tobacco. The qualitative identifications for the dark sun-cured tobacco were all accurate, but the other sample types of two burley samples were mistaken as dark sun-cured tobacco. The qualitative identifications for the oriental tobacco were also all correct; among the other sample types, one dark sun-cured tobacco sample was mistaken as oriental and aromatic tobacco, but the rest were correctly identified.

Table VIII shows that the discriminant rates of the different tobacco types were all above 95%, effectively improving the prediction accuracy of the quantitative NIR analysis. These results also confirm that significantly improving the accuracy of plant regression and quantitative NIR analysis methods is difficult.

Conclusions

This article describes the use of PLS and PLS-DA to establish quantitative single and hybrid NIR spectroscopy models for

Table VI: Prediction results of the total nitrogen of the different models of tobacco

Models*	Mean SEP Value
S-K	0.123
S-Mu	0.214
H-K	0.140
S-Mi	0.210
H-Mi	0.185

*S-K = single models predicting known samples; S-Mu = single models predicting multitype samples; H-S = hybrid models predicting known samples; S-Mi = single models predicting mixed samples; and H-Mi = hybrid models predicting mixed samples.

Table VII: Prediction results of the total alkaloids of the different models of tobacco

Models*	Mean SEP Value
S-K	0.192
S-Mu	0.530
H-K	0.236
S-Mi	0.463
H-Mi	0.141

*S-K = single models predicting known samples; S-Mu = single models predicting multitype samples; H-S = hybrid models predicting known samples; S-Mi = single models predicting mixed samples; and H-Mi = hybrid models predicting mixed samples.

Table VIII: Statistical results of the verification sets of the different types of tobacco

Types	Number of Samples	Minimum	Maximum	Mean	Discriminant Rates (%)
Flue-cured tobacco	30	0.71	1.03	0.91	100
Nonflue-cured tobacco	90	-0.36	0.36	0.03	100
Burley tobacco	30	0.43	1.32	0.84	96
Nonburley tobacco	90	-0.61	0.61	0.06	98
Dark sun-cured tobacco	30	0.53	1.36	0.86	100
Nondark sun-cured tobacco	90	-0.29	0.57	0.06	98
Oriental and aromatic tobacco	30	0.56	1.31	0.88	100
Nonoriental and aromatic tobacco	90	-0.54	0.51	0.02	99

estimating total nitrogen and total alkaloid contents. The means of the SEP from the S-K, S-Mu, S-Mi, H-K, and H-Mi models were 0.123, 0.214, 0.140, 0.210, and 0.185 for total nitrogen and 0.192, 0.530, 0.236, 0.463, and 0.141 for total alkaloids; the error rates were clearly reduced. The single models were more accurate and exhibited stronger predictive ability; thus, these models can be used to predict known sample types. The hybrid models were applied to mixed tobacco. For unknown types of tobacco, the use of qualitative discrimination followed by the S-K model for unknown sample types effectively improved the prediction accuracy of the quantitative NIR models. This technique could constitute a new method for tobacco quality management. The quantitative models are also applicable to the NIR spectroscopic analysis of other plant samples and represent a new discriminant method for other agricultural

products whose appearance is unclear or misleading for various reasons.

References

- (1) W.B. Jin, and Y. Dai, *Tobacco Chemistry* (Tsinghua University Press, Beijing, China, 1994).
- (2) G.D. Zhou, *Dictionary of Chemistry* (Chemical Industry Press, Beijing, China, 2004).
- (3) T. Naes, T. Isaksson, and B. Kowalski, *Anal. Chem.* **62**, 664–673(1990).
- (4) Z. Wang, T. Isaksson, and B.R. Kowalski, *Anal. Chem.* **66**, 249–260(1994).
- (5) V. Centner, and D.L. Massart, *Anal. Chem.* **70**, 4206–4211(1998).
- (6) Y.K. Li, X.G. Shao, and W. Cai, *Chem. J. Chin. Univ.* **28**, 246–249(2007).
- (7) Y.K. Li, X.G. Shao, and W. Cai, *Talanta* **72**, 217–222 (2007).
- (8) C.C. Fagan, C.D. Everard, and K. McDonnell, *Bioresour. Technol.* **102**, 5200–5206 (2011).

- (9) N. Zhao, Z.S. Wu, and Q. Zhang, *Sci. Rep.* **5**, 11647 (2015).
- (10) W. McClure, K. Norris, and W. Weeks, *Beitr. Tabakforsch.* **9**, 13–18 (1977).
- (11) Y. Ma, R. Bai, and G. Du, *Anal. Methods* **4**, 1371–1376 (2012).
- (12) J.T. Diffie, *Pract. Spectrosc.* **13**, 433–473 (1992).
- (13) T. Qiao, J. Ren, and C. Craigie, *Appl. Spectrosc.* **13**, 782 (2015).
- (14) M. Schmutzler, and A. Beganovic, *Food Control.* **57**, 258–267 (2015).
- (15) J.P. Wold, D. Airado-Rodriguez, and A.K. Holtekjølen, *J. Agric. Food Chem.* **65**, 1813–1821 (2017).
- (16) H. Chen, C. Tan, and Z. Lin, *Spectrochim. Acta A Mol. Biomol. Spectrosc.* **189**, 183–189 (2017).
- (17) J.P. Zhang, W.Y. Xie, and R.X. Shu, *Tob. Sci. Technol.* **3**, 37–38(1999).
- (18) A. Tonini, S. Commella, and G. Mellone, *Ann. Ist Spec. Tab.* **99**, 85365 (1981).
- (19) Y. Zhang, Q. Cong, and Y. Xie, *Spectrochim. Acta A.* **71**, 1408–1413 (2008).
- (20) Y. Shao, Y. He, and Y. Wang, *Eur. Food Res. Technol.* **224**, 591–596 (2007).
- (21) S. Wold, M. Sjöström, and L. Eriksson, *Chemometr. Intell. Lab. Syst.* **58**, 109–130 (2001).
- (22) Y.L. Yan, *Technology and Application of NIR Spectra Analysis* (China Light Industry Press, Beijing, China, 2013).
- (23) Y.L. Yan, B. Chen, and D.Z. Zhu. *Qualitative Analysis Methods of Near Infrared Spectroscopy* (Chinese Light Industry Press, Beijing, 2013).
- (24) M. Bevilacqua, and F. Marini, *Anal. Chim. Acta.* **838**, 20–30 (2014).
- (25) W. Lu, Q. Jiang, and H. Shi, *J. Agric. Food Chem.* **62**, 9073–9080 (2014).

Yuqing Yang and **Junhui Li** are with the College of Information and Electrical Engineering at China Agricultural University in Beijing. **Li Ma**, **Guorong Du**, and **Yanjun Ma** are with the Beijing Third Class Tobacco Supervision Station in China. Direct correspondence about this article to Yuqing Yang at 519215532@qq.com, to Junhui Li at caunir@cau.edu.cn, or to Yanjun Ma at 13366036175@189.cn ■

For more information on this topic, please visit our homepage at: www.spectroscopyonline.com

Single-Cell ICP-MS Analysis: Quantifying the Metal Concentration of Unicellular Organisms at the Cellular Level

Accurate quantification of the metal content of individual cells is vital to understanding the uptake mechanisms for risk and dosimetry assessments in environmental and human health sciences. Traditional methods use nominal mass concentrations, missing vital information on metal distribution and the variations that occur at the unicellular level. In this study, we use single-cell inductively coupled plasma–mass spectrometry (ICP-MS) and discuss the steps required for a successful single-cell ICP-MS analysis using a mammalian case study of the uptake of cisplatin into ovarian cancer cells and an ecotoxicological example of the uptake of dissolved and nanoparticulate gold into freshwater algae cells.

Ruth Merrifield, Lauren Amable, and Chady Stephan

All cells need nutrients to survive (1–4). Some of these nutrients are metallic and are absorbed and expelled through the cell membrane from the surrounding media, whether that is an environmental medium (5) or bodily fluid (6). A similar mechanism can lead to the uptake of heavy metal contaminants, nanoparticles (NPs), or metallic drugs that are not beneficial to the cells' survival, and can up-regulate or down-regulate essential cellular metals (7,8).

The manufacture and use of products containing metals, or metallic NPs, has increased in the last few years (9,10). Some of these products have been designed to biologically interact, such as medical (11) or antibacterial products (12,13), while others have not, such as paints, fuel additives, and sunscreens (14). In either case, the interaction of metals on a cellular level is inevitable. These cellular interactions can be advantageous, such as in the delivery of metal-containing drugs into cancer cells (15–17), or harmful, such as the uptake of heavy metals into algal cells (18–20). Quantification of the metal content within cells can be challenging because of the small concentrations contained within the cells, being in the attogram-per-cell range.

There are currently a few average-based methods for measuring or identifying cellular metal content. Total metal content has typically been measured by removing the cells from their culture or exposure media and acid-digesting them for analysis by inductively coupled plasma–mass spectrometry (ICP-MS) (21). This methodology provides the total metal content in a given number of cells and offers an average concentration of metal per cell, by assuming a homogenous distribution. This assumption does not provide a realistic overview, since each individual cell will not accumulate the same amount of ionic or nanoparticulate metal. A more realistic view of NPs and dissolved uptake of metals by cells can be seen in Figures 1a and 1b, respectively, where cells bioaccumulate metals in a non-uniform way with some cells accumulating more metal than others.

Total metal content analysis is often supplemented with techniques such as transmission electron microscopy (TEM), scanning electron microscopy (SEM) (22), and fluorescent tracking (23) to directly visualize metals and metal NPs inside individual cells. These techniques are only qualitative and are prone to artefacts, resulting in false positives.

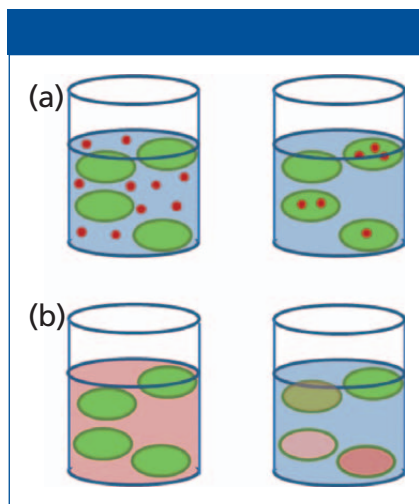


Figure 1: Schematic representation of (a) NPs and (b) dissolved metal uptake by cells.

Table 1: Instrumental conditions for single-cell ICP-MS

Parameter	Single-Cell ICP-MS Value
Spray chamber	Asperon
Nebulizer	Meinhard HEN
Injector	2-mm i.d. quartz
RF power	1600 W
Neb gas flow rate	0.34 mL/min
Make up gas flow	0.7 mL/min
Sample uptake rate	0.01–0.04 mL/min
Dwell time	50 μ s
Settling time	0 s
Analysis time	60 s
Isotopes measured	^{195}Pt
	^{197}Au

Single-cell ICP-MS is a novel ICP-MS technique that directly quantifies the metal content within individual cells at the attogram (ag, 10^{-18} g)-per-cell level. The technique allows for the analysis of single-celled organisms to determine intracellular metal concentrations in both environmental and human health sciences, with minimal sample preparation.

This work focuses on the key considerations, work flow, and sample introduction alterations needed to successfully perform single-cell ICP-MS as well as its application; two examples are provided that highlight the use of this approach in life and environmental sciences. In the first example, we describe the use of single-cell ICP-MS to measure the uptake of cisplatin using cisplatin-sensitive A2780 and cisplatin-resistant CP70 ovarian can-

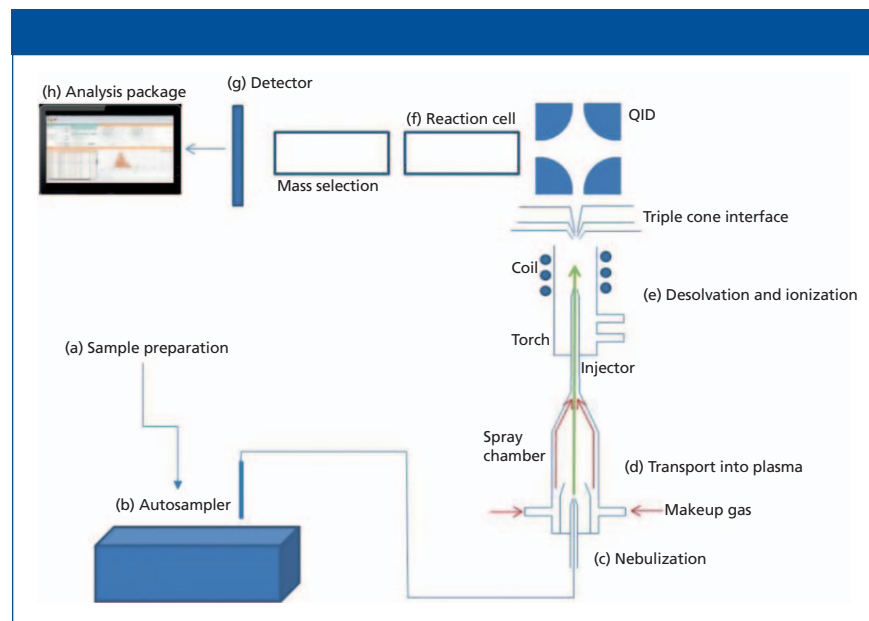


Figure 2: Schematic of optimization and design of single-cell ICP-MS encompassing the following parameters: (a) sample preparation, (b) automated sample injection, (c) aspiration of cell suspensions, (d) spray chamber design, (e) desolvation and ionization, (f) reaction cell gases, (g) sample detection, and (h) sample analysis.

cer cell lines. In the second example, we describe the uptake of dissolved and gold (Au) NPs into various strains of flagellated freshwater algae.

Experimental

Hardware and Instrument Conditions

Introduction: Design Consideration for Single-Cell ICP-MS

Acquiring single-cell suspensions and the introduction of individual intact cells into the plasma are the two biggest challenges for single-cell ICP-MS to be successful. These challenges come with many key components that need to be optimized, as shown in Figure 2, which shows the parts of the single-cell ICP-MS experimental design that must be considered. A more thorough discussion of these parameters follows.

Sample preparation protocols are critical, and need to ensure that cellular integrity is maintained (Figure 2a). Depending on the cell type being analyzed, the requirements for the cell culture vary greatly, and are described in the cell culture section below. Care needs to be taken to ensure that the cells exist as individual cells in suspension (not aggregates), and that treatment of the cells before analysis does not cause cell lysis, resulting in cell fragments entering the plasma, and caus-

ing the appearance of either more events or a false background. Additionally, the media in which cells are grown can range in complexity, ionic strength, and organic content depending on the cell type. Some growth media contains high levels of the metal of interest, which is particularly a problem for intrinsic metal analysis. This background can mask the signal from the cells, making it necessary to resuspend the cells into a media free of that metal.

Automated sampling for single-cell ICP-MS has some specific requirements (Figure 2b). Typically, cells do not remain in suspension and rapidly settle, necessitating the need for cell resuspension before analysis. Additionally, some cells require precise temperatures for survival to reduce the probability of cellular lysis or death. Microsampling and microflow sample delivery to the plasma (flow rates of 20–100 μ L/min) were also required. In this work, a Single Cell Autosampler (PerkinElmer, Inc.) was used. This autosampler is able to mimic pipette-driven agitation to resuspend the cells before sample injection. The sample is then transported into a sample loop before it is introduced into the ICP-MS system via a syringe-driven mechanism delivering microflow rates. It also uses inter-

changeable temperature-controlled sample racks to promote cell survival before analysis.

The sample is injected into the spray chamber through a nebulizer (Figure 2c). The nebulization process applies physical pressure on cells that can result in cell lysis, while the restriction on the sample flow rate means that a high efficiency nebulizer (HEN) is required. The amount of pressure a cell can withstand is highly dependent on cell type, so nebulizer gas flow and sample flow rate of the HEN needs to be evaluated for each cell type to ensure that cell damage does not result from the nebulization process.

Conventional cyclonic spray chambers transport a maximum droplet size of $\sim 4 \mu\text{m}$ to the plasma, with the majority of these being much smaller (28,29). This maximum size is problematic when introducing cells into the plasma, as they are typically 1–100 μm in size. The inefficiency of the cyclonic spray chamber in transporting micrometer-sized particles to the plasma was assessed by comparing the transport efficiency (TE) of 2.5- μm diameter lanthanide-laced polystyrene beads to that of 60-nm Au NPs. The TE for these beads was only 0.03% (± 0.01), compared to a TE of around 7% for 60-nm Au NPs, meaning that micrometer-sized particles are less likely to reach the plasma than NPs. This TE difference highlights why this design is not a viable option for single-cell ICP-MS. A new linear-pass spray chamber (Asperon, PerkinElmer) was developed to increase cell transport, decrease collisions of the cells with the chamber wall, and limit the amount of solvent entering the plasma, thereby improving stability and cell viability (Figure 2d). A dual make-up gas inlet was positioned to create a tangential flow in the spray chamber, creating a laminar flow that prevents cells from colliding with and sticking to the chamber walls and ensuring maximum transport of the cells to the plasma. Using this spray chamber, the TE experiments using the lanthanide-laced polystyrene beads and Au NPs were repeated. A transport efficiency of 33% for both nano- and micrometer-sized particles was obtained, showing equal transportation through the chamber (37). This result demonstrated that the Asperon spray chamber did not differentiate between droplet sizes and ensured optimal delivery to the ICP-MS plasma.

After successfully transporting intact individual cells to the plasma, the plasma atomizes and ionizes the cells (Figure 2e). The resulting ions travel as ion plumes through the ion optics of the instrument, including passing through the reaction cell (Figure 2f), which can either be run in standard mode or reaction mode, to reduce interferences. The ion of interest is then mass-selected by a quadrupole before detection. The detector (Figure 2g), along with advanced data processing, is capable of fast data acquisition with dwell times down to 10 μs and zero settling time, thereby providing an accurate measurement of the total metal content within each individual cell. Finally, the analysis of the data (Figure 2h) was achieved using dedicated software that allows for real-time visualization of the individual cell events, providing a peak-area distribution of the cell population during data acquisition (Figure 3). The peak areas are then converted into mass of metal per cell (attograms per cell), and displayed in a histogram of mass per cell against frequency of that mass range.



Figure 3: Conversion of metals within individual cells to mass per cell histogram using the Syngistix single-cell application software module.

Instrumental Conditions

Analyses were performed with a Nexion ICP-MS using the Syngistix Single Cell application software module for data collection and processing (PerkinElmer, Inc.). Instrumental conditions are shown in Table I. Sample introduction was accomplished with a high-efficiency nebulizer coupled to an Asperon spray chamber.

ICP-MS Methods

Cancer Cell Experiments

Ionic platinum standards (1, 2, and 3 ppb) were prepared in phosphate-buffered saline (PBS) to matrix-match the cell samples. The transport efficiency was determined using

Certified
Reference
Materials for
Instrument
Qualification

The widest range:
Deep UV to Infra-red
Up to 3.5 Absorbance
NIST Traceable
ISO 17034 Reference
Material Producer
ISO/IEC 17025 accredited supplier
Lifetime Guarantee
Fast Recalibration Service
Meet all International
regulatory Standards



Starna

Starna Cells, Inc.
PO Box 1919 Atascadero, CA 93423

Phone: (800) 228-4482 USA or (805) 466-8855 outside USA
sales@starnacells.com www.starnacells.com

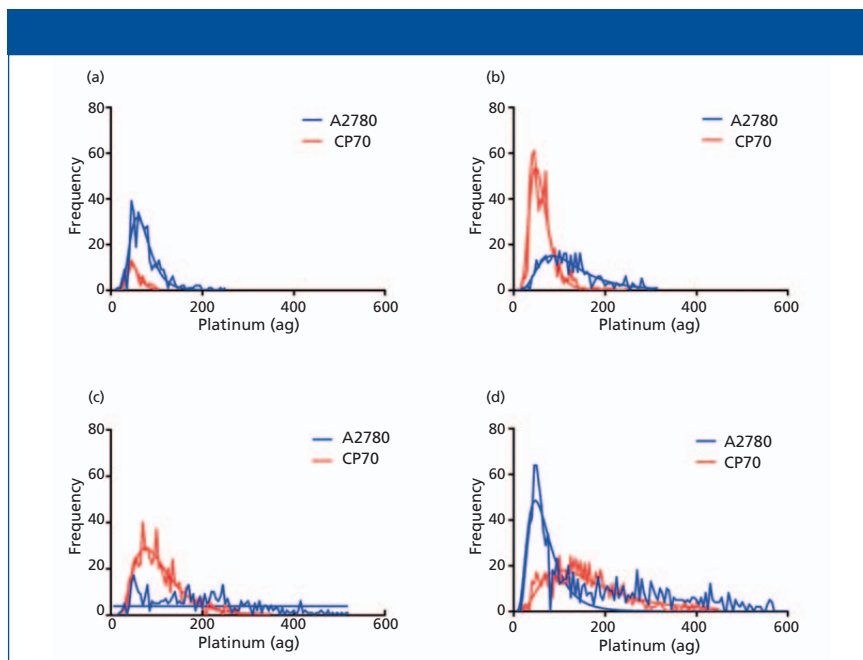


Figure 4: Single-cell ICP-MS plots demonstrating the change in cellular platinum distribution for cell lines A2780 (blue) and A2780/CP70 (red) after (a) 1-, (b) 2-, (c) 4-, and (d) 8-h post 30 μM cisplatin treatment.

60-nm gold nanoparticles (National Institute of Standards and Technology [NIST]) in PBS.

Algae Experiments

Calibrations were performed with both ionic-dissolved and NP standards. The ionic calibration was performed with 1, 2, and 3 ppb Au, and the NP calibration was done using 10-, 30-, and 60-nm Au NPs (NIST 8011, 8012, and 8013, respectively), prepared at 50,000 part/mL. All standards were prepared in the algae media to matrix-match the cell suspensions. Transport efficiency was determined using the 60-nm Au NPs.

Cell Cultures

Cancer Cell Culture and Cisplatin Treatment

Ovarian cancer cell lines A2780 and A2780/CP70 were used in all experiments. Cells were grown in RPMI 1641 media (Gibco) supplemented with 10% fetal bovine serum (FBS, Gibco), insulin (Sigma-Aldrich), l-glutamine, and pen/strep (Gibco) under 5% CO_2 at 37 °C. Cisplatin was resuspended at 1 mg/mL in sterile saline and vigorously shaken for 30 min before treatment. Cells were treated with 30 μM cisplatin and samples collected at intervals of 1, 2, 4, and 8 h post-treatment. For analysis, cells were washed twice with

PBS and collected using the non-enzymatic cell dissociation solution Cellstripper (Corning). Cells were centrifuged at 500g for 10 min. The supernatant was discarded, and the cells were resuspended in 1 mL PBS, filtered through a 70- μm nylon mesh, and quantitated by hemocytometer counting. Cells were diluted in PBS to a final concentration of 100,000 cells/mL and kept on ice until analysis.

Algae Cell Culture and Metal Gold (Au) Treatment

Stock cell cultures were kept at 20 °C and exposed to light-dark cycles of 12 h each. They were gently agitated each day and fresh media added twice a week to ensure healthy growth conditions. Cell cultures were prepared at concentrations of 200,000 cells/mL and exposed to either dissolved Au (1 ppb) or Au NPs (60 nm NPs, NIST 8013, 500,000 part/mL). The cells were exposed to the solutions 1 h after the initiation of the light cycle. Each exposure study was run in triplicate at 20 °C for 3 h under an ultraviolet (UV) lamp.

During the exposure, 1-mL aliquots were removed periodically for analysis. The cell number in the cultures was measured via hemocytometer at each time point. Before analysis, the algae cells were separated from the exposure

media and washed with fresh media three times. Each wash cycle consisted of centrifuging the cells for 15 min at 300 g and resuspending in 1 mL of the fresh culture media (containing no NP or ionic Au). After the three washes, the cell recovery was $43.8 \pm 8.6\%$.

The supernatant from the first cycle was analyzed for changes in the metal exposure and the washed cells were analyzed for metal cellular content. Both of these conditions are important for environmental risk assessment because metals and metal NPs undergo transformations under environmental conditions (35), while cells may be more susceptible to taking up metals that have transformed versus those that have not (36). T-tests were performed to measure the statistical differences between samples.

Results and Discussion

Cancer Cell Treatment with Cisplatin

Cisplatin is a platinum-based chemotherapy drug used to treat a variety of cancers. The effectiveness of cisplatin therapy is related to its ability to form DNA-Pt adducts, which results in cell death (30). Understanding how a population of cancer cells takes up cisplatin dictates the response to the chemotherapy. There are three molecular mechanisms of cisplatin resistance: increased DNA repair, increased cytosolic inactivation, and altered cellular accumulation (30), including decreased cellular uptake or decreased cellular export. The paired ovarian cancer cell lines A2780 and A2780/CP70 were chosen as a model to demonstrate the capability of single-cell ICP-MS. A2780 is the cisplatin-sensitive cell line from which the cisplatin-resistant A2780/CP70 cell line was derived. The A2780/CP70 cells were shown to have an increased resistance to cisplatin (IC_{50} 30 μM) in comparison to A2780 cells (IC_{50} 3 μM). Reduced cisplatin uptake and increased DNA repair are the molecular mechanisms by which the A2780/CP70 cell line mitigates resistance to cisplatin (31). Thus, this paired cell line, with altered cisplatin uptake, is an attractive model for the development of measuring cisplatin at the level of a single cell.

Time course experiments were performed on A2780 and A2780/CP70 cell lines to analyze how the uptake of cis-

platin changed over time within the cell population. Both cell lines were treated with 30 μM cisplatin for 1, 2, 4, and 8 h. Both cell lines displayed an overall heterogeneous distribution of cisplatin uptake, yet differences were observed between the cell lines (Figure 4). At 1 h post-cisplatin treatment, both cell lines had measurable levels of intracellular cisplatin, although the A2780 cells had a higher number of platinum-containing cells than the A2780/CP70 cells. Two hours after cisplatin treatment, both cell lines displayed an increase in the number of cells containing platinum and higher intracellular cisplatin levels. With the A2780 cells showing a larger increase compared to the A2780/CP70 cell line. At 4 h post-cisplatin treatment, the A2780 cellular population displays a wide variation in intracellular cisplatin levels. This trend continued at 8 h where highly varied cisplatin levels are observed. Interestingly, a new population of cells containing low cisplatin levels became prominent. This development suggests that there was a small population of cells that did not immediately import cisplatin and therefore displayed a partial resistance. In contrast, a steady increase in the intracellular levels of cisplatin and the distribution of cisplatin within the cell population was observed at 4 and 8 h post-treatment in the A2780/CP70 cell population.

Results from the time-course experiments are summarized and graphed by plotting the mean intensity for each cell line, as shown in Figure 5. As expected, the cisplatin-sensitive A2780 cells have increased cisplatin uptake in comparison to the cisplatin-resistant A2780/CP70 cells over time. These results were concordant with what has been observed previously in the literature—A2780 cells accumulate more platinum than the cisplatin-resistant cell line A2780/CP70 (31). However, when the results were plotted in this traditional manner, the intracellular variation of the cellular population was not apparent.

Algae Exposures to Au

Accurately measuring exposure levels and cellular uptake of metallic products in environmental systems can be challenging because of either low lev-

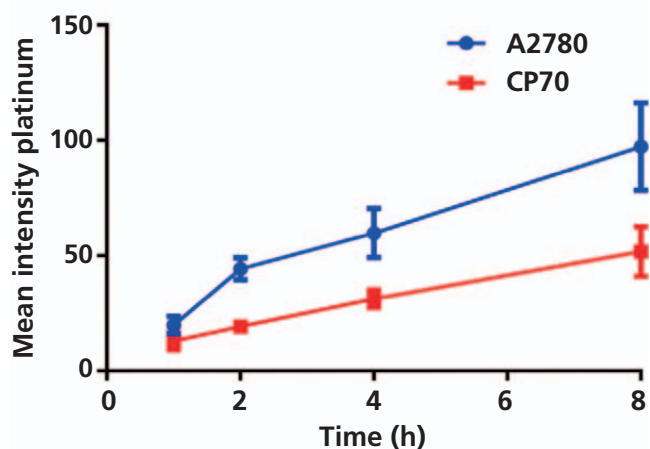


Figure 5: Mean amount of platinum per cell for the two cell lines over an 8-h period.

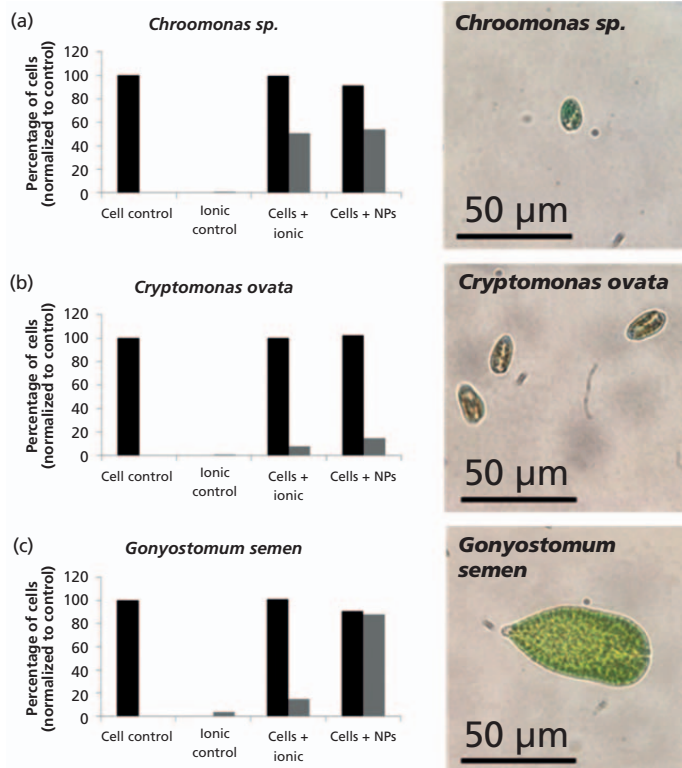


Figure 6: Percentage of cells containing Au after 3 h of exposure (a) *Chroomonas sp.*, (b) *C. ovata*, and (c) *G. semen*.

els (32–34) or biological diversity. We used single-cell ICP-MS to quantify the metal exposure concentration, NP transformations in the media, and the metal distribution within the cells.

There algal strains (*Chroomonas sp.*, *Cryptomonas ovata*, and *Gonyostomum semen*) were exposed to both 60-nm Au NPs and dissolved Au (Figure 6). The

black bars represent the total number of cells in the culture, as measured by hemocytometer, and the gray bars represent the number of those cells that contain Au metal after 3 h of exposure (all percentages were normalized to the original number of cells at 0 h). The results show that different algae cell lines take up dissolved and NPs Au differently.

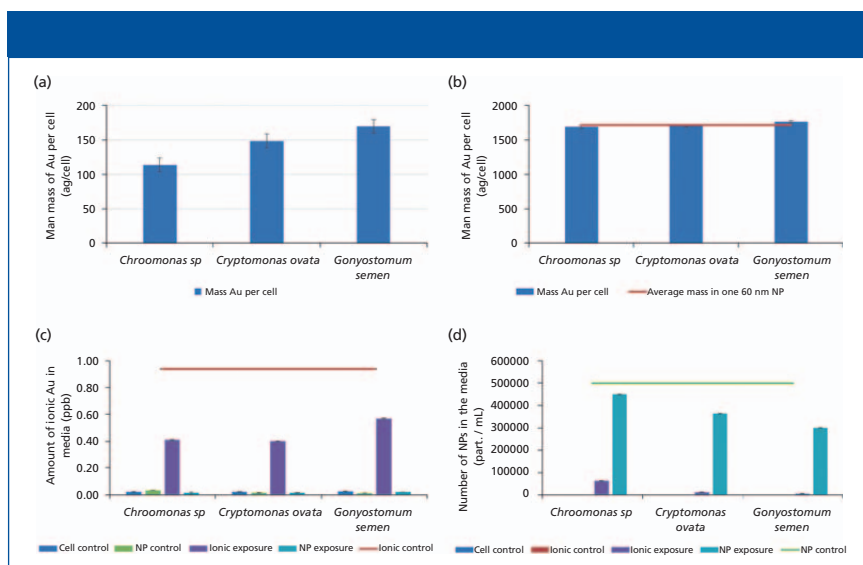


Figure 7: Mass of Au per cell after 3 h of exposure to (a) ionic exposures (blue bars) and (b) NP exposures (blue bars), compared to amount of metal in a single NP (dashed red line). The average amount of Au metal in the media for control cells, ionic control, NP control, ionic exposure, and NP exposure after 3 h: (c) ionic exposures compared to the ionic control (red line) and (d) number of NPs compared to NP controls (green line).

Chroomonas sp. takes up both dissolved and NP Au quickly and at the same rate, with 50–60% of the cells containing Au metal in both cases. In comparison, *C. ovata* takes up significantly less Au in both the dissolved and NP form over this short time period, but takes up both almost equally, with about 15–20% of the cell population containing Au in both exposures. However, the largest cells, *G. semen*, take up significantly more NPs than dissolved Au, with around 95% of the total cell population containing Au NPs, and only 15% containing dissolved Au. This result shows that the uptake of Au is dependent both upon the algal species and the form of the metal to which is it exposed. These results also highlight that not all cells within a population necessarily take up Au, indicating that the uptake of a given metal may be heterogeneous as described in Figure 1, where this information is overlooked when using traditional techniques.

The average mass of Au per cell was quantified using single-cell ICP-MS for both dissolved and NP exposures (Figures 7a and 7b), while the concentration and form of Au left in the media was determined by measuring the first supernatant during the washing stages (Figures 7c and 7d). Figure 7a shows that after 3 h of exposure to

dissolved Au, the average mass of Au per cell was found to be greatest in *G. semen* (around 165 ag/cell) and least in *Chroomonas sp.* (110 ag/cell) even though fewer *G. semen* cells contained Au (Figure 6c).

In contrast, cells that were exposed to NPs contained the same amount of Au, around 1770 ag/cell (Figure 7b). These results were not significantly different between algal species or the amount of Au contained in a single NP (dashed line in Figure 7b), showing that most cells contained a single NP. Cells containing multiple NPs (n) would cause the appearance of populations of cells with average masses of $n \times 1770$ (that is, 3540 ag/cell for 2 NPs/cell, 5310 ag/cell for 3 NPs/cell, and so on).

Because of transformations (such as NP dissolution, reprecipitation, or aggregation), uptake into cells, and adsorption to the container walls, the NP or dissolved exposure concentration can change dramatically with time. This is an important factor to quantify because it can change the exposure conditions, reducing the amount of metal available to the cells. Figure 7c shows that the amount of ionic dissolved Au in the media after 3 h of exposure to algae cells was reduced compared to the ionic control. Dissolved Au is only sig-

nificantly present in the ionic exposures and ionic control. The ionic concentration decreased by approximately 60% in exposed *Chroomonas sp.* and *C. ovata*, and about 40% in the *G. semen* exposure study. The number of NPs in the media for the exposures and controls can be seen in (Figure 7d). In this case, between 10% and 40% of the NPs have been removed from the media after 3 h of exposure to cells with variations observed between cell lines. Although no transformations have occurred (mass/NP is not significantly different from controls), the exposure concentration has significantly reduced, even within the first 3 h of exposure, resulting in a dramatic change in the amount of NPs left in the media for the cells to interact with and leading to a reduced exposure concentration. This effect would be even greater over the duration of a typical toxicity test of 72 h.

Conclusion

The development of single-cell ICP-MS has, for the first time, offered the ability to accurately quantify the metal concentrations within individual cells, providing new information on the mean metal content and the variation within a cell population. This method was shown to be a vital tool for assessing the specific uptake of metals by ovarian cancer cells and fresh water algae alike.

It was demonstrated that the uptake of cisplatin by the cisplatin-sensitive/resistant paired ovarian cancer cell lines A2780 and A2780/CP70, was heterogeneous within the cell populations. Cisplatin uptake increases over time in both cell lines. However, cisplatin uptake into the resistant A2780/CP70 cell line is comparatively less than the sensitive A2780 cell line. This study has shown that single-cell ICP-MS is a powerful analytical tool that has great potential in the development of new strategies for drug advancement. These strategies include the evaluation of new mechanisms to increase cisplatin uptake in cells, and the identification of novel pathways that influence cellular cisplatin uptake and depuration.

Single-cell ICP-MS has been shown to accurately quantify both the changes in exposure concentration and dose

(amount taken-up) of dissolved and NP Au to a variety of fresh water algal species. The uptake was dependent on both the metal phase and algal species. The scope of information gained by single-cell ICP-MS studies will aid in the risk assessment of metals and the development of regulations that govern NP concentrations in the environment, by providing the only current method which allows for the direct quantification of the mass of a metal within individual cells.

Acknowledgments

This research was funded in part by the Intramural Research Program of the National Institute of Health (NIH), National Institute on Minority Health and Health Disparities (NIMHD), and the SmartState Centre for Environmental Nanoscience and Risk (CENR), at the University of South Carolina.

References

- (1) D.K. Button, *Microbiol. Rev.* **49**(3), 270–297 (1985).
- (2) M.G.V. Heiden, L.C. Cantley, and C.B. Thompson, *Science* **324**(5930), 1029–1033 (2009).
- (3) P. Vaupel, F. Kallinowski, and P. Okunieff, *Cancer Res.* **49**(23), 6449–6465 (1989).
- (4) M. Honti, V. Istvanovics, and A.S. Kovacs, *Sci. Total Environ.* **408**(20), 4712–4721 (2010).
- (5) W.G. Sunda and S.A. Huntsman, *Sci. Total Environ.* **219**(2–3), 165–181 (1998).
- (6) E.C. Foulkes, *Proc. Soc. Exp. Biol. Med.* **223**(3), 234–240 (2000).
- (7) T.A. Davis, B. Volesky, and A. Mucci, *Water Res.* **37**(18), 4311–4330 (2003).
- (8) M.L. Guo, H.Z. Sun, H.J. McArdle, L. Gambling, and P.J. Sadler, *Biochemistry* **39**(33), 10023–10033 (2000).
- (9) F. Piccinno, F. Gottschalk, S. Seeger, and B. Nowack, *J. Nanopart. Res.* **14**(9), 1–11 (2012).
- (10) T.Y. Sun, F. Gottschalk, K. Hungerbuehler, and B. Nowack, *Environ. Pollut.* **185**, 69–76 (2014).
- (11) M. Akrami, S. Balalaie, S. Hosseinkhani, M. Alipour, F. Salehi, A. Bahador, and I. Haririan, *Sci. Rep.* **6**, 12 (2016).
- (12) Y. Li, J. Niu, C. Zhang, Z. Wang, M. Zheng, and E. Shang, *Progress in Chemistry* **26**(2–3), 436–449 (2014).
- (13) V. Shah, S. Shah, H. Shah, F.J. Rispoli, K.T. McDonnell, S. Workeneh, A. Karakoti, A. Kumar, and S. Seal, *Plos One* **7**(10), e47827 (2012).
- (14) W.J. Stark, P.R. Stoessel, W. Wohlleben, and A. Hafner, *Chem. Soc. Rev.* **44**(16), 5793–5805 (2015).
- (15) J. Park, N.R. Kadasala, S.A. Abouelmagd, M.A. Castanares, D.S. Collins, A. Wei, and Y. Yeo, *Biomaterials* **101**, 285–295 (2016).
- (16) V. Khare, A. Singh, G. Mahajan, N. Alam, S. Kour, M. Gupta, A. Kumar, G. Singh, S.K. Singh, A.K. Saxena, D.M. Mondhe, and P.N. Gupta, *Eur. J. Pharm. Sci.* **92**, 183–193 (2016).
- (17) N.D. Eljack, H.Y.M. Ma, J. Drucker, C. Shen, T.W. Hambley, E.J. New, T. Friedrich, and R.J. Clarke, *Metallomics* **6**(11), 2126–2133 (2014).
- (18) Y.G. Jiang, Y.L. Zhu, Z.L. Hu, A.P. Lei, and J.X. Wang, *Ecotoxicology* **25**(7), 1417–1425 (2016).
- (19) J.F. Cheng, H.C. Qiu, Z.Y. Chang, Z.M. Jiang, and W.K. Yin, *Springerplus* **5**, (2016).
- (20) F. Perreault, A. Oukarroum, S.P. Mellegrari, W.G. Matias, and R. Popovic, *Chemosphere* **87**(11), 1388–1394 (2012).
- (21) A.E. Egger, C. Rappel, M.A. Jakupec, C.G. Hartinger, P. Heffeter, and B.K. Keppler, *J. Anal. At. Spectrom.* **24**(1), 51–61 (2009).
- (22) N.S. Taylor, R. Merrifield, T.D. Williams, J.K. Chipman, J.R. Lead, and M.R. Viant, *Nanotoxicology* **10**(1), 32–41 (2016).
- (23) O.S. Wolfbeis, *Chem. Soc. Rev.* **44**(14), 4743–4768 (2015).
- (24) H.Q. Doan, G.M. Chinn, and R.R. Jahan-Tigh, *J. Invest. Dermatol.* **135**(12), 3204–3204 (2015).
- (25) N. Leelatian, D.B. Doxie, A.R. Greenplate, B.C. Mobley, J.M. Lehman, J. Sinnaeve, R.M. Kauffmann, J.A. Werkhaven, A.M. Mistry, K.D. Weaver, R.C. Thompson, P.P. Massion, M.A. Hooks, M.C. Kelley, L.B. Chambless, R.A. Ihrle, and J.M. Irish, *Cytometry Part B-Clinical Cytometry* **92**(1), 68–78 (2017).
- (26) D.R. Bandura, V.I. Baranov, O.I. Ornaty, A. Antonov, R. Kinach, X.D. Lou, S. Pavlov, S. Vorobiev, J.E. Dick, and S.D. Tanner, *Anal. Chem.* **81**(16), 6813–6822 (2009).
- (27) S.C. Bendall, G.P. Nolan, M. Roederer, and P.K. Chattopadhyay, *Trends Immunol.* **33**(7), 323–332 (2012).
- (28) G. Schaldach, L. Berger, I. Razilov, and H. Berndt, *J. Anal. At. Spectrom.* **17**(4), 334–344 (2002).
- (29) H. Matusiewicz, M. Slachcinski, B. Almagro, and A. Canals, *Chem. Anal. (Warsaw, Pol.)* **54**(6), 1219–1244 (2009).
- (30) L. Amable, *Pharmacol. Res.* **106**, 27–36 (2016).
- (31) R.J. Parker, A. Eastman, F. Bostickbruton, and E. Reed, *J. Clin. Invest.* **87**(3), 772–777 (1991).
- (32) F. Gottschalk, E. Kost, and B. Nowack, *Environ. Toxicol. Chem.* **32**(6), 1278–1287 (2013).
- (33) I. Mahapatra, T.Y. Sun, J.R.A. Clark, P.J. Dobson, K. Hungerbuehler, R. Owen, B. Nowack, and J. Lead, *J. Nanobiotechnol.* **13**(1), 1–14 (2015).
- (34) F. Gottschalk, T. Sun, and B. Nowack, *Environmental Pollution* **181**, 287–300 (2013).
- (35) R.C. Merrifield, C. Stephan, and J. Lead, *Environ. Sci. Technol.* **51**(6), 3206–3213 (2017).
- (36) M.N. Croteau, S.K. Misra, S.N. Luoma, and E. Valsami-Jones, *Environ. Sci. Technol.* **45**(15), 6600–6607 (2011).
- (37) R.C. Merrifield, C. Stephan, and J.R. Lead, *Environ. Sci. Technol.* **52**(4), 2271–2277 (2018).

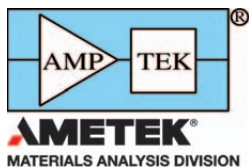
Ruth Merrifield is with the Center for Environmental NanoScience and Risk (CENR), Department of Environmental Health Sciences, Arnold School of Public Health, at the University of South Carolina in Columbia, South Carolina and PerkinElmer, Inc., in Shelton, Connecticut. **Lauren Amable** is with the Division of Intramural Research, National Institute on Minority Health and Health Disparities, National Institutes of Health in Bethesda, Maryland. **Chady Stephan** is with PerkinElmer, Inc. Direct correspondence to: Chady.Stephan@perkinelmer.com or Ruth.Merrifield@perkinelmer.com ■

For more information on this topic, please visit our homepage at: www.spectroscopyonline.com

VENDOR PERSPECTIVES

WHAT DO YOU THINK IS ONE OF THE BIGGEST CHALLENGES CURRENTLY FACING ATOMIC SPECTROSCOPY?

ATOMIC SPECTROSCOPY



The applications for X-ray fluorescence (XRF) analysis continue to grow globally. The technique is very powerful and versatile, and generally speaking, very easy to use. Amptek has seen significant advancements in food analysis (ppm level analysis of Cd in Rice, for example, in China) and in on-line processing. The biggest challenge for manufacturers is finding qualified scientists and engineers that understand XRF to improve algorithms to achieve the low levels they require (in the case of food analysis) and being able to find partners to integrate solutions for on-line analysis. Amptek's scientists and engineers provide a tremendous amount of support on-line, by phone, and on-site, but the demand is great and growing!

David A. Clifford, director, sales & marketing, Amptek

Demand for information on the distribution of elements in food, water, soil, and air continues to be driven by regulations that push for lower limits not only on concentrations, but also on the chemical and physical forms of these elements. This translates into the need for faster, more reliable, and easier-to-use instrumentation, while ease of interfacing with separation techniques is becoming a must to identify the chemical forms of various elements in these matrices. Furthermore, the fate of nanoparticles in the environment and their impact on human health is a key driver for more fundamental research in atomic spectroscopic detection.



Fadi Abou-Shakra, ICP-MS portfolio director, PerkinElmer Inc.



We find that we are continuously pushing the limits of our instruments trying to detect lower and lower levels of elements of interest in high matrix samples. The high matrix samples challenge instrumentalists to find corrections for interferences and design method sequences to limit carry over. In our ICP-MS instruments, we employ a variety of gases to eliminate different interferences. We enjoy working closely with our customers to design and test custom products to address these difficult demands.

SPEX CertiPrep Inorganic Chemists

VENDOR PERSPECTIVES

WHAT DO YOU THINK IS ONE OF THE BIGGEST CHALLENGES CURRENTLY FACING MASS SPECTROMETRY?

MASS SPECTROMETRY



One big challenge for mass spectrometry in a world driven toward the Internet of Things (IoT) and Cloud approaches is enabling effective modes to transfer, store, and access, to process or view the large sets of data generated by modern high-resolution accurate mass instruments for batches of samples. Such data are relevant in many areas including chemical synthesis optimizations, synthetic biology, xenobiotic metabolism as well as metabolomics and proteomics.

Graham McGibbons, Director of Strategic Partnerships, ACD/Labs

VENDOR PERSPECTIVES

WHAT DO YOU THINK IS ONE OF THE BIGGEST CHALLENGES CURRENTLY FACING MOLECULAR SPECTROSCOPY?

MOLECULAR SPECTROSCOPY

The biggest challenge facing any spectroscopy method is the inherent complexity of the information gathered and the necessity to convert this information into data that is understandable and usable by end-users. Unfortunately, at the end-user site, personnel expertise and capacity have been reduced due to cost-cutting and merger activities at the production sites. The answer ABB offers to this challenge comes in the form of pre-calibrated, robust, and easy-to-maintain OA-ICOS analyzers and FT-IR instruments embedded with the ABB Ability service, a global cloud-based service that receives individual analyzer health information, maintains calibrations, and centralizes related information.



Dr. Michael Kleimann, industry manager, Life Sciences and Specialty Chemicals, ABB Measurement & Analytics

Optical fiber probes enable the use of key spectroscopy methods for remote reaction monitoring and process control in industry, but may be also used for tissue analysis in clinical diagnostics. To secure minimal invasive but complete cancer removal, a medical fiber probe can assist in tumor margin definition by fluorescence or molecular spectroscopy methods: Raman scattering, IR-absorption, or diffuse NIR-reflection. While multi-spectral fiber systems will help to select the most sensitive, specific, and accurate methods or their combination—the special spectral fiber sensors will be developed for specific tumors.



Viacheslav Artyushenko, managing director, art photonics GmbH

VENDOR PERSPECTIVES

WHAT DO YOU THINK IS ONE OF THE BIGGEST CHALLENGES CURRENTLY FACING MOLECULAR SPECTROSCOPY?

MOLECULAR SPECTROSCOPY

A current challenge for molecular spectroscopy is developing enhanced in-situ techniques and tools for characterizing catalytic materials and processes. Catalysis is essential in the production of more than 70% of today's fuels and other chemical products. Thus, optimizing catalysts is a critical need. Harrick Scientific produces advanced spectroscopic sampling devices and reaction cells that are proven tools for catalysis research. These include temperature- and pressure-controlled chambers for in-situ Operando catalysis and photochemistry studies, adaptable to FT-IR, UV-vis, Raman, and X-ray spectrometric techniques. A key challenge is to develop in-situ spectroscopy reaction cells that more closely mimic the real-world conditions of large-scale reaction processes.



Jeff Christenson, marketing and sales manager, Harrick Scientific

In today's Raman spectroscopic applications, optical filters play a crucial role in collecting the wavelength-shifted Raman scattered photons from the Rayleigh scattered light at the same wavelength as the excitation laser source. Accessing as much of the Raman fingerprint of the molecule of interest as possible requires filters that provide "more signal with less background." Iridian's industry-leading series of ultra-steep edge-pass filters and narrow notch filters addresses these Raman spectroscopic needs. The Nano-edge LPFs with cut-offs of $<26\text{ cm}^{-1}$ (corresponding to 0.2% of the laser wavelength), together with high transmittance $> 90\%$ and deep blocking $> \text{OD } 6$, and the Wide Angle Edge tunable ultra-steep edge filters, provide the premium solution for your Raman instruments.



Hongbai Lao, sales engineer, Iridian Spectral Technologies



One of the challenges in molecular spectroscopy is the analysis of complex materials, such as those in the biological, clinical, or food industries, where interfering fluorescence is a factor in the analysis. Many researchers use laser wavelengths in the region towards the infrared, even though there is a trade-off between a weakened Raman intensity with reduced fluorescence. Raman systems with efficient optics and NIR lasers are extremely important. JASCO is also developing software with machine learning and artificial intelligence to make it easier for the user to identify measurement position, optimize parameters, and to accurately identify components and visualize sample matrices.

Carlos Morillo, PhD, Raman & IR applications scientist, JASCO

VENDOR PERSPECTIVES

WHAT DO YOU THINK IS ONE OF THE BIGGEST CHALLENGES CURRENTLY FACING MOLECULAR SPECTROSCOPY?

MOLECULAR SPECTROSCOPY

With recent advances, most instrumentation produced today for molecular spectroscopy is as powerful, connected, and simple to use as it's ever been. This is great news for researchers and developers, who thrive by having greater access to these sophisticated techniques.



One significant challenge is being able to apply knowledge and insight to the data this new instrumentation captures, so that greater understanding—"better" answers, if you will—is the result. This transformation will include more effective use of tools such as algorithm development, artificial intelligence, and machine learning.

Rob Morris, knowledge manager, Ocean Optics



It's always a challenge to translate research to the real world. For very good reasons, proof of concept work in new applications is done under controlled conditions and with prepared samples. This doesn't always mimic real-world conditions, either for the samples or the instruments. It's much more difficult to extract meaningful spectroscopic data from complex mixtures with overlapping spectra or interfering peaks from contaminants and organic matrices like tissue and soils. Highly repeatable data over a range of operating conditions is very important. It is also essential that we develop new mathematical methods of data extraction and analysis.

Cicely Rathmell, VP Marketing, Wasatch Photonics

A major challenge for molecular spectroscopy, and confocal Raman imaging in particular, is that there's a staggering variety of sample materials and substrates being looked at. A high-resolution Raman microscope can quickly detect and acquire spectra with exceptional sensitivity. These spectra must then be identified and located in the image for a comprehensive understanding of the sample. Databases can help sift through potential materials while data analysis software can link them to the image. A seamlessly-integrated instrument consisting of hardware, database, and post-processing functionality all controlled through an intuitive user interface is the most effective tool for addressing that challenge.



Olaf Hollricher, managing director, Research and Development, WITec GmbH

PRODUCTS & RESOURCES

FT-NIR laboratory analyzer for biodiesel

ABB's MB3600-CH30 FT-NIR laboratory analyzer for biodiesel is designed for determining biodiesel properties in final product and mid-batch biodiesel samples from vegetable oil transesterification reactors. According to the company, the analyzer uses a transmission sampling method with disposable glass vials.

ABB Measurement & Analytics,

Quebec, QC, Canada;
www.abb.com/analytical

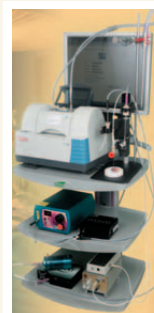


Multispectral fiber MSF system

The multispectral fiber MSF system from art photonics GmbH is designed to allow comparison of four key spectroscopy methods and selection of the best one for a distinct application, or the design of a combi-probe for an optimal data fusion from two or more methods. According to the company, tiny fiber probes are used for diagnostics of biofluids and tissues in vitro, ex vivo, and in vivo.

art photonics GmbH,

Berlin, Germany;
www.artphotonics.com



Lasers for Raman spectroscopy

New wavelengths are available on Cobolt's 08-01 series of 457-, 473-, 515-, 660-, and 1064-nm lasers, complementing available wavelengths of 405, 532, 561, and 758 nm. According to the company, these single-frequency and narrow-linewidth lasers are suitable for Raman spectroscopy applications. **Cobolt AB, a part of Hübner**, Solna, Sweden;
www.coboltlasers.com



Microwave sample preparation application note

An application note on single reaction chamber (SRC) microwave digestion in pharmaceutical testing laboratory environments is available for download from Milestone. According to the company, the application note, titled "Application of SRC Technology in Pharmaceutical Testing Lab Environments," outlines implementation of microwave-assisted digestion using SRC technology by a leading global provider of laboratory testing services to increase sample preparation efficiencies and lower costs. **Milestone, Inc.**, Shelton, CT; <https://milestonesci.com/usp-232-233-compliance/>



IR spectrometer

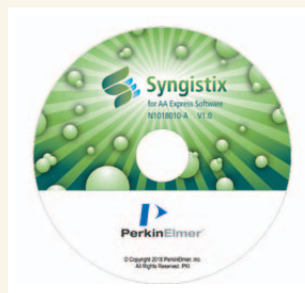
The Ocean MZ5 miniature mid-infrared attenuated total reflectance (MIR-ATR) spectrometer from Ocean Optics is designed as a compact alternative to FT-IR for applications that include chemical discrimination, food and flavorings analysis, environmental testing, and scientific research. According to the company, the spectrometer has a measurement range of 1818–909 cm^{-1} (5.5–11 μm). **Ocean Optics**, Largo, FL;
oceanoptics.com/product/mz5-atr-mir-spectrometer



Atomic spectroscopy software

PerkinElmer's Syngistix for AA Express software is designed for use with the company's PinAAcle 900H flame and furnace AA spectrometer. According to the company, the software provides a streamlined workflow with three steps to results.

PerkinElmer,
Waltham, MA;
www.perkinelmer.com



Raman pharmaceutical analyzer

Renishaw's RA802 pharmaceutical analyzer is designed as a compact benchtop Raman imaging system for the pharmaceutical industry. According to the company, it determines API and excipient domain statistics, allowing efficient formulation of tablets.

Renishaw,
Hoffman Estates, IL;
www.renishaw.com/ra802



UV-vis spectrophotometer

The UV-1900 UV-vis spectrophotometer from Shimadzu is designed for analysis in foods, pharmaceuticals, life sciences, chemistry, and electronics applications. According to the company, the spectrophotometer has a color touch panel that allows users to control with a finger or the provided stylus pen, and it includes validation functions that are compliant with the United States Pharmacopeia and the European Pharmacopoeia.

Shimadzu Scientific Instruments, Columbia, MD;
www.ssi.shimadzu.com



Fluorimeter

Spectrolight's FWS fluorimeter is designed for use in a range of applications. According to the company the fluorimeter integrates its tungsten halogen lamp, Mighty Light, with its Flexible Wavelength Selector to provide a tunable, monochromatic beam for excitation.

Spectrolight, Inc.,

Irvine, CA;

www.spectrolightinc.com/product-category/fluorimeter



Raman spectrometers

Wasatch Photonics' Raman spectrometers are designed for materials identification, authentication, trace analysis, and biomedical applications. According to the company the spectrometers have a spectral range of 2000–4300 cm^{-1} , and are available for 405-, 532-, 633-, 785-, 830-, and 1064-nm excitation, as probe and free-space models and integrated laser systems.

Wasatch Photonics,

Durham, NC;

www.wasatchphotonics.com



Raman microscopy reaction chamber

Harrick's high-temperature reaction chamber for Raman microscopy is designed with a cell that has a single horizontal window and a low profile for compatibility with Raman instrumentation. According to the company, the chamber allows environments with temperature up to 910 °C and with pressures ranging from 10^{-6} to 2200 Torr.

Harrick Scientific Products, Inc.,

Pleasantville, NY;

www.harricksci.com



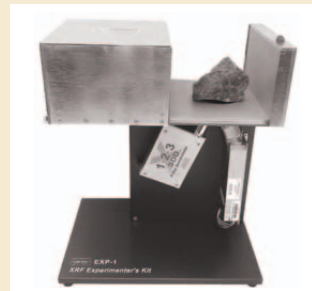
XRF kit

Amptek's XRF kit is designed to help users quickly begin doing elemental analysis via X-ray fluorescence. According to the company, the kit includes the company's X-123 complete spectrometer with a FAST SSD or SSD detector, a Mini-X USB Controlled X-ray tube, XRF-FP QA software, a sample enclosure, and test sample.

Amptek, Inc.,

Bedford, MA;

www.amptek.com



Raman analyzer

The RamanRXN2 Multichannel analyzer from Kaiser is designed to provide high-resolution, research-grade Raman spectra on a portable platform for process development monitoring and control. According to the company, a single analyzer can collect Raman data from four channels, addressable by fiber-optic probes capable of direct in situ liquid or solid measurements in applications ranging from raw materials identification to process control in a manufacturing environment.

Kaiser Optical Systems, Inc.,

Ann Arbor, MI; www.kosi.com



Benchtop X-ray diffractometer

The MiniFlex benchtop X-ray diffractometer from Rigaku is designed as a general-purpose instrument that can perform qualitative and quantitative analysis of polycrystalline materials. According to the company, an optional graphite monochromator, coupled with the standard scintillation counter, maximizes sensitivity by optimizing peak-to-background ratios.

Rigaku Corporation,

Tokyo, Japan;

www.rigaku.com/en/products/xrd/miniflex



Polymer fluorescent references

Starna's second-generation polymer fluorescent references are designed for wavelength calibration and the monitoring of instrument performance in fluorescent applications. According to the company, the new references are based on new proprietary dyes and provide increased stability and resistance to photobleaching, allowing for their use as relative photometric intensity references.

Starna Cells, Inc.,

Atascadero, CA;

www.starnacells.com



Raman opioid analysis application note

An application note titled "FT-Raman: An Invaluable Addition to the Forensic Arsenal to Combat the Opioid Epidemic" is available from Thermo Fisher Scientific. The application note reportedly describes the advantages of using Fourier transform Raman spectroscopy to detect and identify fentanyl and other illicit drugs.

Thermo Fisher Scientific,

Madison, WI;

www.thermofisher.com/spectroscopy





**Precision NMR
Sample Tubes &
Sampling Accessories**

Quality and value you can rely on!

Standard and Special Applications

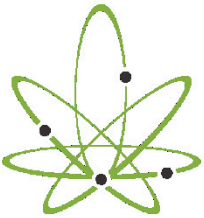


New Era Enterprises, Inc.
Ph: 1-800-821-4667 Fax: 1-856-697-8727
cs@newera-spectro.com www.newera-spectro.com

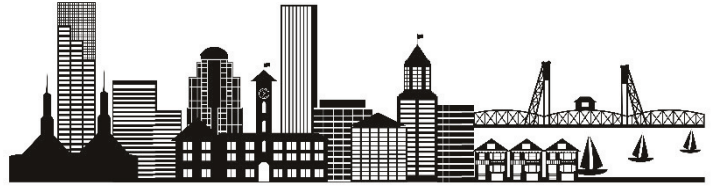
Ad Index

ADVERTISER	PG#	ADVERTISER	PG#
ABB, Inc.....	7, 41	Milestone.....	5
ACD/Labs.....	41	New Era Enterprises, Inc.....	46
Amptek.....	3, 40	Ocean Optics, Inc.....	CV2, 43
art photonics GmbH.....	15, 41	Ondax, Inc.....	19
Edinburgh Instruments.....	25	PerkinElmer Corporation.....	40, CV4
FACSS.....	11	PIKE Technologies.....	17
Harrick Scientific Corporation.....	9, 42	Rigaku GMG.....	8
Iridian Spectral Technologies.....	42	SPEX CertiPrep.....	40
JASCO, Inc.....	42	Starna Cells, Inc.....	23, 35
jCanna, Inc.....	CV3	Wasatch Photonics, Inc.....	43
LECO Corporation.....	21	WITec GmbH.....	43

Use Promo Code **CSC25** for 25% Off Registration!!!



CANNABIS
SCIENCE
CONFERENCE



August 27-29, 2018



Portland, Oregon



OREGON Oregon
Convention
Center



The World's Largest Cannabis Science Conference

returns to downtown Portland for an incredible gathering of analytical scientists, medical professionals, patients, cannabis industry experts and novices interested in learning more about cannabis science!

Sponsorship and exhibition opportunities are available. Please contact Andrea at andrea@jcanna.com for more info.

CANNA BOOT CAMP • ANALYTICAL, CULTIVATION & MEDICAL TRACKS



CannabisScienceConference.com



@CannabisScienceConference



@CannabisScienceConference



**ANY MATRIX
ANY INTERFERENCE
ANY PARTICLE SIZE**

NexION 2000 ICP-MS: Triple quad power meets single quad versatility.

Trace metals in food, nanomaterials in water, impurities in everything from pills to electronic components: These are the sweet spot for the NexION® 2000 ICP-MS. Its sample introduction technology lets you run samples with up to 35% total dissolved solids. Plus, its interference

removal capabilities give you the best detection limits for your application. And it delivers superior analysis times and single particle/cell detection capability – at least 10x faster than competitive systems. So the NexION 2000 ICP-MS is up to the most important challenge of all: *Yours.*



NexION 2000 ICP Mass Spectrometer

For more information,
visit perkinelmer.com/NexION2000